



City Research Online

City, University of London Institutional Repository

Citation: Li, Z. & Tsavdaridis, K. D. (2022). Limited-damage 3D-printed interlocking connection for timber volumetric structures: Experimental validation and computational modelling. *Journal of Building Engineering*, 63, 105373. doi: 10.1016/j.jobee.2022.105373

This is the published version of the paper.

This version of the publication may differ from the final published version.

Permanent repository link: <https://openaccess.city.ac.uk/id/eprint/28978/>

Link to published version: <https://doi.org/10.1016/j.jobee.2022.105373>

Copyright: City Research Online aims to make research outputs of City, University of London available to a wider audience. Copyright and Moral Rights remain with the author(s) and/or copyright holders. URLs from City Research Online may be freely distributed and linked to.

Reuse: Copies of full items can be used for personal research or study, educational, or not-for-profit purposes without prior permission or charge. Provided that the authors, title and full bibliographic details are credited, a hyperlink and/or URL is given for the original metadata page and the content is not changed in any way.

City Research Online:

<http://openaccess.city.ac.uk/>

publications@city.ac.uk

Journal Pre-proof

Limited-damage 3D-printed interlocking connection for timber volumetric structures:
Experimental validation and computational modelling

Zhengyao Li, Konstantinos Daniel Tsavdaridis



PII: S2352-7102(22)01379-1

DOI: <https://doi.org/10.1016/j.jobe.2022.105373>

Reference: JOBE 105373

To appear in: *Journal of Building Engineering*

Received Date: 16 June 2022

Revised Date: 6 September 2022

Accepted Date: 3 October 2022

Please cite this article as: Z. Li, K.D. Tsavdaridis, Limited-damage 3D-printed interlocking connection for timber volumetric structures: Experimental validation and computational modelling, *Journal of Building Engineering* (2022), doi: <https://doi.org/10.1016/j.jobe.2022.105373>.

This is a PDF file of an article that has undergone enhancements after acceptance, such as the addition of a cover page and metadata, and formatting for readability, but it is not yet the definitive version of record. This version will undergo additional copyediting, typesetting and review before it is published in its final form, but we are providing this version to give early visibility of the article. Please note that, during the production process, errors may be discovered which could affect the content, and all legal disclaimers that apply to the journal pertain.

© 2022 Published by Elsevier Ltd.

Limited-Damage 3D-Printed Interlocking Connection for Timber Volumetric Structures: Experimental Validation and Computational Modelling

Zhengyao, Li¹ and Konstantinos Daniel Tsavdaridis^{2*}

¹School of Civil Engineering, Faculty of Engineering and Physical Sciences, University of Leeds, Woodhouse Lane, LS2 9JT, Leeds, UK

²Department of Engineering, School of Science and Technology, City, University of London, Northampton Square, EC1V 0HB, London, UK

*Corresponding author: Konstantinos.tsavdaridis@city.ac.uk

Abstract

Cross laminated timber volumetric construction (CLTVC) is an innovative construction technology that combines the sustainability of timber and the efficiency of modular construction, as opposed to conventional construction. However, the connection installing methods of CLTVC, such as fastening, are laborious with limited accessibility for connection installations, thus hindering the application of CLTVC in mid- and high-rise structures. Therefore, a new way of connecting CLT modules by sliding and stacking is explored herein with a proposed damage-control interlocking connection system, aiming to provide a more efficient assembly solution to CLTVC that does not require onsite screwing. Quasi-static monotonic and cyclic test, and numerical analyses were conducted to assess the mechanical performance of the proposed connections, which possessed adequate translational stiffness and strength of the proposed connections. The connections' ability to control deformation – damage is moved away from timber and the embedded fasteners, was also well demonstrated in the test, as both screws and timber remained mostly intact after testing. The proposed connection design showcases a new concept of modules' assembly in volumetric construction with higher efficiency and flexibility; meanwhile demonstrates the potential in reducing the permanent damage to structural materials during service life and enabling reuse.

1. Introduction (more recent studies, new interlocking connections and their limitations)

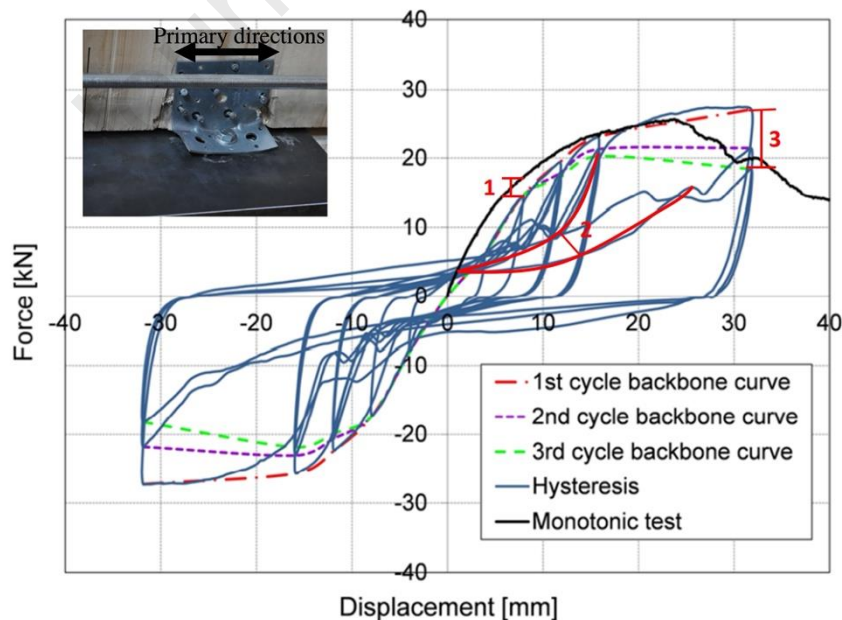
1.1 Multi-storey timber volumetric construction

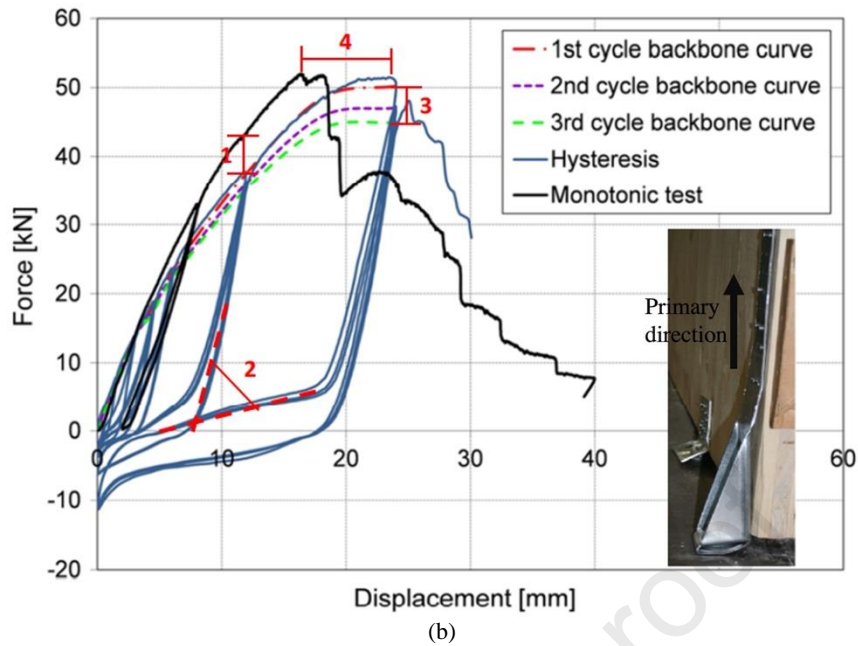
Volumetric construction is an emerging modern method of construction (MMC) that has the highest degree of prefabrication (~95%) [1] with the main structure and other building accessories such as cladding, internal finishes and MEP services all being manufactured and assembled into flat modules in factories (offsite manufacturing - OSM) before being transported to sites for the final assembly. With the advent of automation and the future factories (the fourth industrial revolution), better quality and higher precision of assembly work compared to the on-site manual operation can be ensured in volumetric construction. Being able to combine the sustainability of timber materials and the efficiency

38 of the OSM, volumetric timber construction is considered as one of the direct solutions to the growing
 39 demand in affordable urban accommodation as well as the high carbon footprint problem own to the
 40 construction industry [2]. Yet, this construction technology is limited to mid- and low-rise structures
 41 [2], and the current trend of building tall volumetric timber structures imposes new challenges on the
 42 wind and seismic resistances of such structural systems, requiring further investigations on varied
 43 aspects of VTC; for example updates on design strategy in standards, high-performing connection
 44 systems and assembly tools, as well as the development of more accurate numerical modelling methods
 45 [3] for the confident delivery of secured high-rise volumetric timber structures.

46 1.2 Conventional timber connection systems for multi-story VTC

47 Among all the currently available forms of timber volumetric structures, the Cross Laminated Timber
 48 (CLT) volumetric structure that employs load-bearing CLT panels, has somewhat better potential over
 49 others (e.g., Framed Volumetric Structures and Structural Insulated Panels, SIPs) to be used for tall
 50 buildings due to the high stiffness of CLT. However, suitable connections for this structural system still
 51 lack sufficient investigation, as it is a relatively new construction technology. In volumetric
 52 construction, the connections between modular units, also known as inter-module connections, are
 53 critical to both the project efficiency and the overall structural performance of the buildings, as they
 54 link prefabricated modular units together on-site to form the entire structure and are designed to transfer
 55 horizontal and uplift forces from the wind and seismic actions. Previous quasi-static tests on CLT
 56 panelised systems [4] [5] and shake table tests on full-scale low-rise CLT buildings [6] [7] indicated
 57 that structures made of CLT panels generally demonstrated high strength and stiffness with most of the
 58 deformation and energy dissipation being processed in connections and friction between timber panels.
 59 Therefore, the proposal of high-performing connections is crucial to the realisation of high-rise
 60 volumetric CLT structures with improved wind and seismic performances.





61 Fig. 1. Typical CLT connections (a) angle bracket and (b) hold-down and their representative monotonic and cyclic
 62 responses and failure modes on the primary working directions [8]

63 Angle brackets and hold-downs (Fig. 1) are the commonly used shear and tensile connections in timber
 64 construction, which are originally designed for post-and-beam timber structures, so they are not fully
 65 applicable in CLTVC. Some well-known disadvantages of these connection systems in both
 66 construction and structure aspects currently limit their application in high-rise CLT volumetric
 67 structures. To name a few:

68 1.2.1 Incompatibility with CLTVC and low construction efficiency

69 The limited accessibility is a widely recognised challenge in volumetric construction. The installation
 70 of conventional timber connections requires external access, while accessibility for inter-module
 71 connections has long been a key challenge in volumetric construction [9], especially when CLT
 72 modules become enclosed as panelised structures, which makes the inter-module connections in
 73 CLTVC entirely inaccessible (Fig. 2). Consequently, in some CLT volumetric structures [2, 10], the
 74 inter-module connections are absent and the lateral resistance of the structure is provided by the friction
 75 between modules or the additional structural reinforcing systems, such as steel frames and concrete
 76 cores. This method is commonly adopted in low-rise CLTVC and the inaccessibility of inter-module
 77 connections is treated as one of the main obstacles to achieving tall CLT volumetric structures with
 78 sufficient lateral stiffness, considering the importance of inter-module connections in defining the
 79 integrity and stability of volumetric structures.

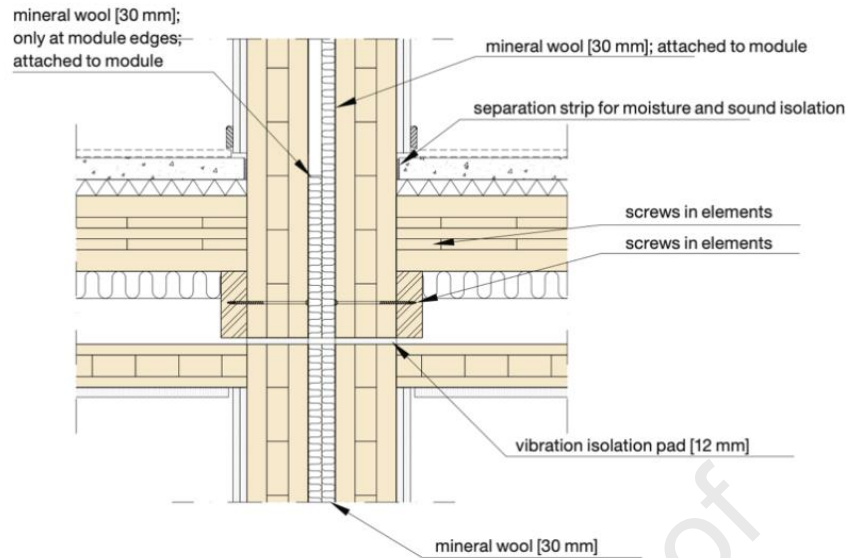


Fig. 2. Illustration of inaccessible inter-module connection between CLT modules [11]

1.2.2 Insufficient mechanical properties

According to the published experimental studies [8, 12], both angle brackets and hold-downs are characterised by high stiffness and strength but insufficient ductility (belonging to L or M ductility class as prescribed in EC8 [13]) in their primary directions (Fig. 1(a)&(b)). In the cyclic tests on conventional connections, several hallmarks can be observed (Fig. 1): (1) the reduced maximum strength at each step than that in monotonic test at the same displacement amplitude, (2) the stiffness degradation happens at load reversals, (3) the strength degradation occurs during the repeated cycles at the same displacement, (4) the delayed attainment of maximum strength in cyclic test compared to monotonic test.

The above-mentioned features are attributed to the cavities around fasteners formed by the crushing of timber and the deformation of fasteners during loading, which damage the capacity of surrounding timber and are highly unfavourable to the seismic design of high-rise structures, as they make the connection cyclic behaviours unpredictable and reduce the structure's capacity of energy dissipation during seismic events [14].

In addition, as the connection is the governing factor of the timber structures' ductility, the common concept of designing ductile timber structures is achieved by increasing the number of connections while using small-diameter fasteners. Large number of conventional connections with slender fasteners are therefore commonly adopted in large timber structures to achieve desired structural capacity (Fig. 3), which leads to time-consuming on-site fastening work that negatively impacts the project progress. This also limits the maximum reclamation and the reuse of timber components at the end-of-life of buildings, as the removal of nails and screws is labour-intensive and can damage the structural material [15]. Another concern of using small-diameter fasteners is the high stress they introduce on timber after experiencing significant deformation at the later stage of loading, which can pinch through the fibres before the capacity in timber is fully developed (Fig. 4(a)), causing sudden drop in connection strength and great residual displacement even after the removal of the external loading. This can be considered as brittle failure and cause irreversible damage to the structural elements, which results in difficulties in structural maintenance and should be avoided in connection design.



Fig. 3. Numerous angle brackets used on a single CLT shear wall to achieve sufficient capacity and ductility

1.2.3 Insufficient accuracy in analytical models for connection capacity calculation

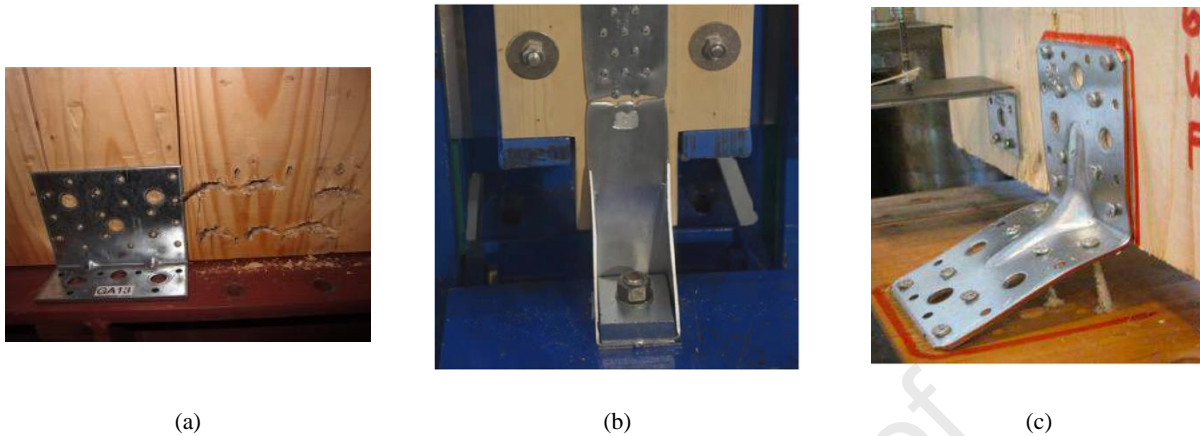
Comparison studies between analytical models and experiment results were conducted in previous research [8, 12], which indicated that the existing analytical models for timber connections provide conservative predictions on connection strength but seems to significantly overestimate the stiffness (up to 9 times higher according to the study of Gavric and Fragiaco [8]). One potential source of errors in the analytical models can be the assumption of brittle elements (timber) and ductile elements (fasteners and steel plate) working independently, with the embedding strength of timber and the yield moment of fastener being considered separately in calculations. This is because typical timber connections are composite structures, in which deformation happens simultaneously in ductile and brittle elements when loaded (Fig. 4(b)&(c)). Hence, considering the strength of different components independently and ignoring the composite effect when estimating the overall capacity of the connection could lead to significant differences between the actual strength and the calculated value. The much bigger actual strength of the embedded fasteners than the design value that was estimated with Johansen's theory in EC5 [16], and the overestimations of the stiffness and strength of the brittle elements due to the much greater scattering of timber material properties than steel material [17], can also lead to inaccurate estimations in connection design, which may cause non-ductile failure modes in connections (e.g., splitting of timber) [8, 12].

The afore-mentioned factors also affect the overstrength method that widely adopted in the research and practice of timber structures, which is developed by Jorissen and Fragiaco (Eq.1) [18] based on capacity-based design method to ensure the full activation of all ductile elements before the non-ductile area enters the plastic stage [19]. In this method, an overstrength factor γ_{Rd} accounting for all possible factors that may lead to unexpected high strength in ductile elements ($R_{d,ductile}$) (underestimated material strength, potential strain hardening and contribution of steel plate at large deformations) is introduced in the design strength of brittle elements ($R_{d,brittle}$) (Eq.1).

$$\gamma_{Rd} R_{d,ductile} \leq R_{d,brittle} \quad (1)$$

This factor is defined as the ratio of the 95th-percentile strength distribution to the analytical design strength capacity of the connection [18]. The inaccurate estimations of analytical models can lead to the

138 adoption of inappropriate overstrength factors, which may further result in the overdesign of structural
 139 material or the unfavourable connection behaviours.



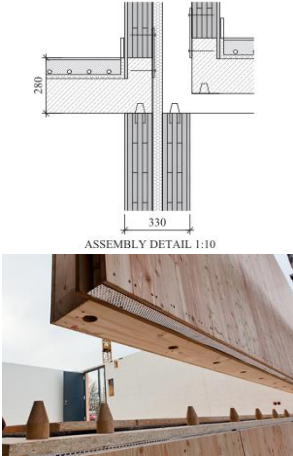
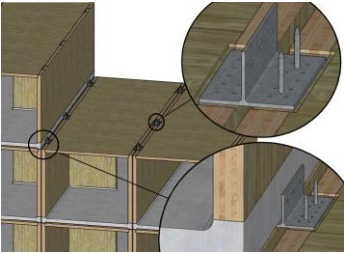
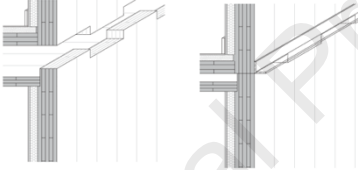
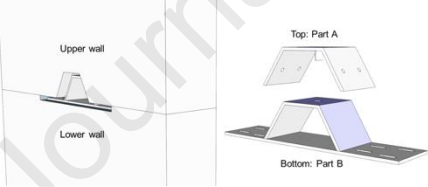
140 Fig. 4. Possible deformation modes in timber connections: (a) localised deformation on fasteners with timber fibres being cut
 141 through [8] (b) brittle failure on metal flange (c) combination of bending of plate, splitting of timber and withdrawal of
 142 screws [20]

143 1.3 Innovative connection systems

144 To address the limited accessibility of inter-module connections in volumetric construction, a new way
 145 of assembling flat modules using interlocking techniques was explored in previous research [21, 22].
 146 These conceptual studies demonstrate the potential of interlocking technique in achieving
 147 replaceability, adaptability and dismantlability in volumetric structures. This technique was also
 148 employed in the design of some recently proposed connection prototypes for CLT volumetric structures,
 149 as summarised in Table 1. These new connections eliminate the onsite manual operation in CLTVC
 150 needed for screwing, so that the access to inter-module connections is not required, and better
 151 construction efficiency and accuracy can be achieved. Similar interlocking design can also be observed
 152 in some new connections proposed for CLT panelised structure (Table.1). These recent developments
 153 enrich the importance of interlocking technique in CLT connection systems for efficient construction
 154 and upgraded structural performance. However, the listed interlocking connections for CLTVC are all
 155 bespoke connection solutions proposed for specific projects, while a universal interlocking connection
 156 solution for CLTVC has not yet been proposed. And these bespoke connections all require special
 157 modifications on CLT panels for the fitting of connections, which limit their applications in other CLT
 158 volumetric structures.

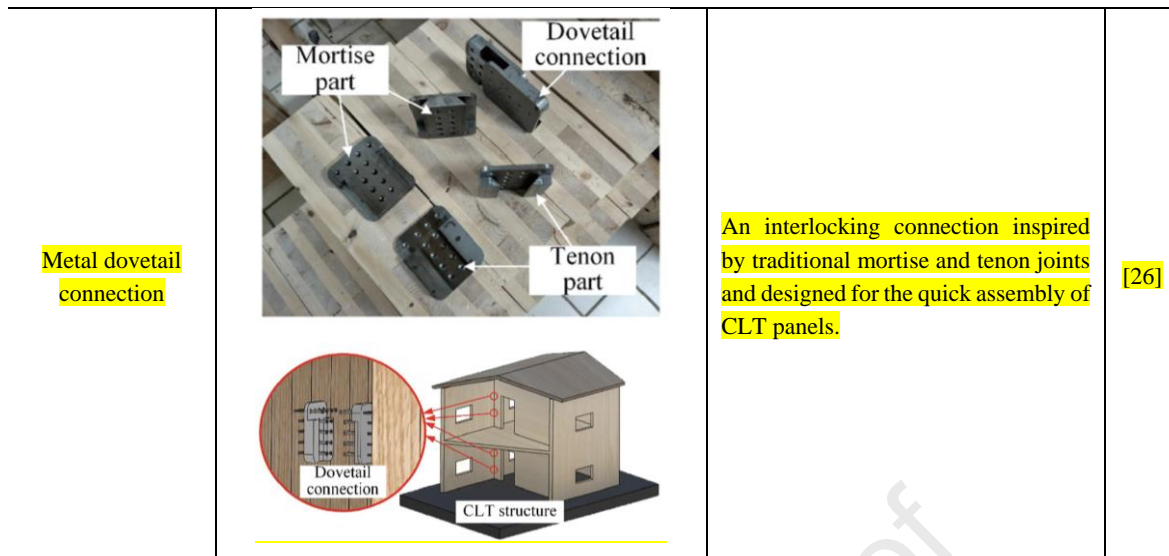
159 **Table 1.** List of innovative interlocking connection systems for CLT structures

Name	Connection Fig.s	Comments	Ref
Novel connections for CLT volumetric structures			

<p>Heidelberg Student Accommodation</p>	 <p>ASSEMBLY DETAIL 1:10</p>	<p>A bespoke interlocking inter-module connection for the easy installation of CLT flat modules.</p>	<p>[2]</p>
<p>Jakarta Hotel</p>		<p>A steel T-shaped angle plate with pins for the accurate alignment and translational constraints of modules</p>	<p>[23]</p>
<p>Moxy Modular Hotels (Marriott)</p>		<p>A specially designed notched CLT panel used as the side wall of modules and the inter-module connection for the easy on-site modules assembly.</p>	<p>[2]</p>
<p>A novel inter-module horizontal connection proposed by the University of British Columbia</p>		<p>A replaceable inter-module connection to achieve good energy dissipation and limit plastic deformation in timber.</p>	<p>[24]</p>

Interlocking connections for CLT panelised structures

<p>LOCK Connection from Rothoblaas Ltd.</p>		<p>A concealed, interlocking wall-to-floor connection for CLT structures. The Lock Connection is attached on the surfaces or edges of wall and floor CLT panels, so the floor panels can be slid into the right positions to connect with wall panels, eliminating on-site fastening work.</p>	<p>[25]</p>
---	---	--	-------------



160

161 In some novel connections [27-31] designed for CLT panelised structures, another commonly adopted
 162 design strategy is to introduce an individual ‘weak component’ in the connections to control the plastic
 163 deformation. By applying capacity-based design to strengthen timber and fasteners, this design strategy
 164 can efficiently isolate timber from deformation and localise the deformation within the additional metal
 165 connectors. In this way, much improved strength and ductility can be achieved in connections with
 166 reduced risks of brittle failure, considering the limited ability of timber to deform plastically. A similar
 167 approach is also widely adopted in the recent proposals of dissipator [32-35] for CLT structures.

168 2. Novel Interlocking Connection System for CLT Modules

169 2.1 Concept of the interlocking connection

170 In order to achieve enhanced structural performance in multi-storey CLT volumetric structures and
 171 simplify the module assembly process, a novel interlocking inter-module connection system is herein
 172 proposed. This connection system consists of both vertical and horizontal connections that can be pre-
 173 installed onto CLT modules in the factory (off-site) (Fig. 5(a)). It is suitable for most of the module
 174 specifications, as it requires no further modification on panels for the fitting of connection, which can
 175 greatly simplify and standardise the structural design process and become available to the entire market.
 176 Owing to its interlocking feature, the modules can be accurately assembled on-site by sliding and
 177 stacking without the need for additional tooling and special operations (Fig. 5(b)&(c)), so the on-site
 178 assembly of modules will no longer be constrained by the access of inter-module connections and the
 179 erection process of CLT volumetric structures can be significantly sped up.

180

181

182

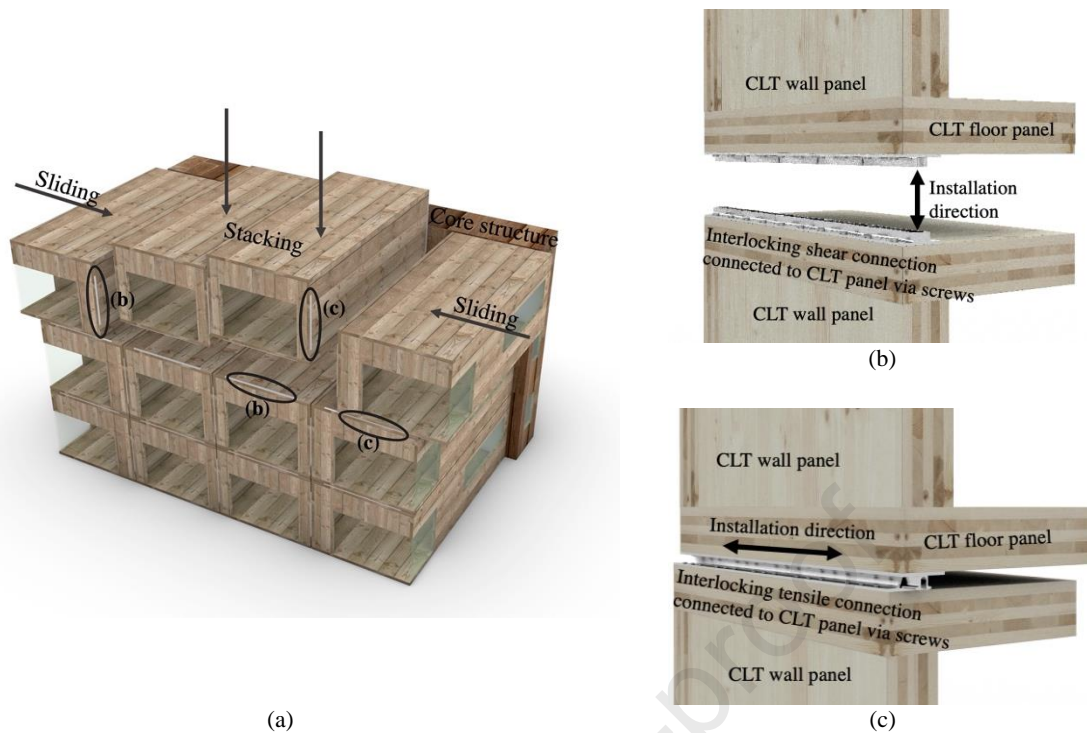
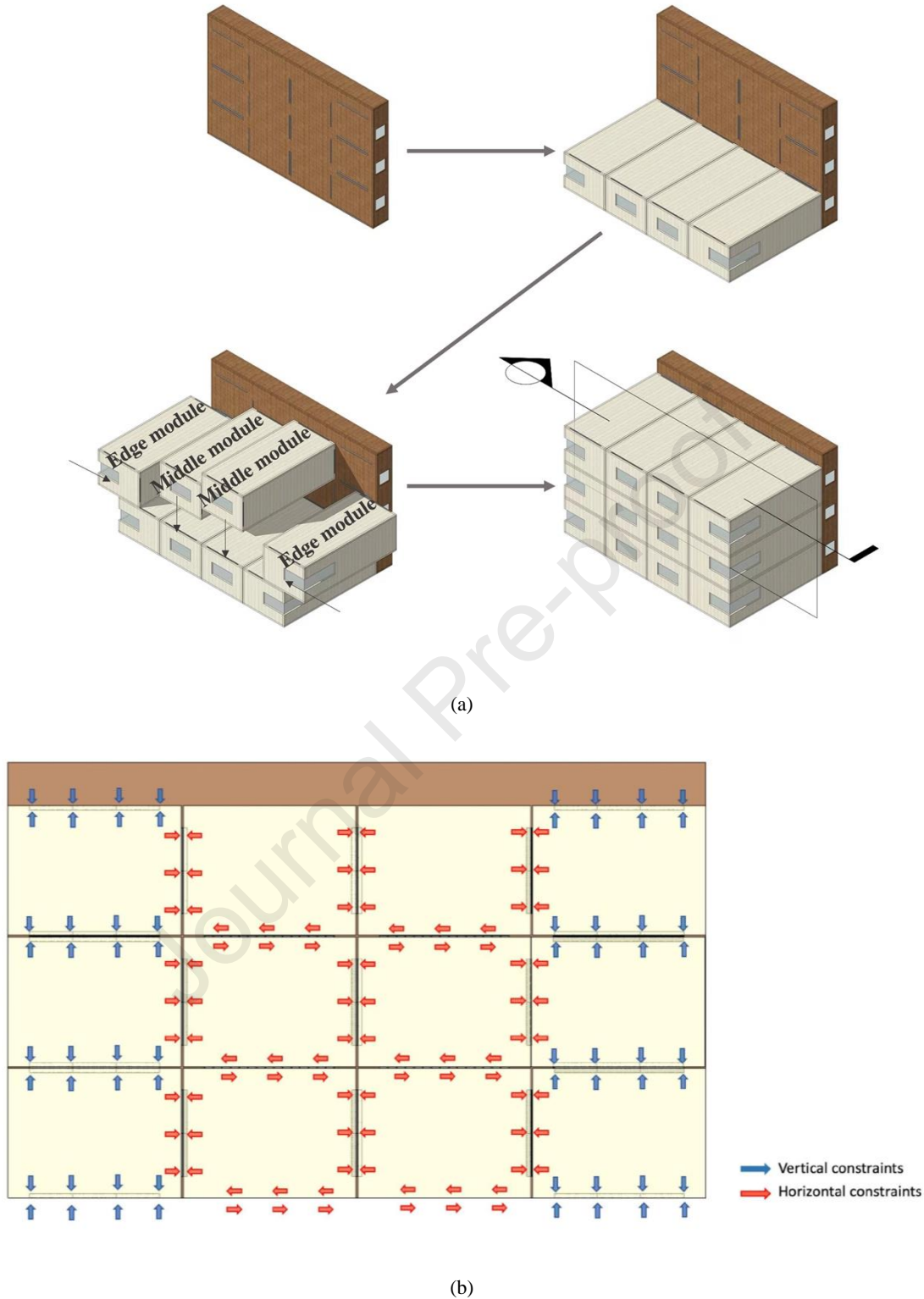


Fig. 5. Overview of the novel interlocking connection system for VTC: (a) Locations of connections in a CLT volumetric structure and the assembly of CLT modules with the pre-installed connections (b) the stacking of interlocking shear connection (c) the sliding of interlocking tensile connection

183
184
185

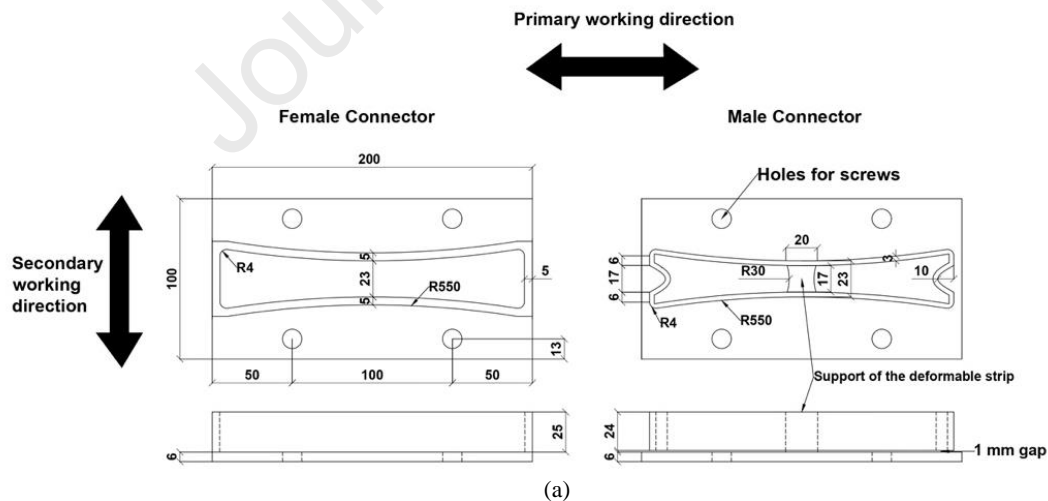
186 Due to the interlocking technique, both shear and tensile connections of this new system are not fully
187 rigid in the installation direction and are designed to transmit shear or tensile forces only (Fig. 6(b)).
188 After assembly, the movement of connectors can be locked by simple end-locking systems (i.e.
189 extended plates with holes welded on the ends of the connectors, through which fasteners can fix two
190 connectors). The full integration of constraints on the structure in both horizontal and vertical directions
191 is achieved by the strategic placement of modules. In the CLTVC with interlocking connections as
192 illustrated in Fig. 6, the core structure used as lift shaft or staircase is first constructed with preinstalled
193 connections. Following the arrangement of the connections on the core structure, the flat modules with
194 pre-installed connections can simply slide over or be stacked into the correct positions (Fig. 6(a)). The
195 illustrated strategic assembly can form a continuous vertical reinforcement along the edge modules and
196 a horizontal reinforcement along the middle modules (Fig. 6(b)), resisting the uplifting and inter-storey
197 drift caused by external forces. The continuous reinforcement provided by this connection strip design
198 can also minimise load concentration on CLT panels as well as provide a certain amount of bending
199 resistance, though bending moment is often neglected in CLT building design due to the high in-plane
200 stiffness of CLT panels. This kind of edge-supporting connection system, as proved by the previous
201 numerical analysis on similar interlocking connection [21], can help achieve enhanced integrity in
202 volumetric structures. When damage happens in the connection units of one of the modules, the entire
203 structures can remain stable with little movement and require no need for immediate replacement,
204 because alternative load path can form along the edges of the remained modules, reassuring that the
205 performance requirements is still satisfied. In addition, located at the exterior surface of modules, the
206 interlocking connections are invisible from the interior of flats and can be protected from the external
207 environment by the façade after the completion of the project.

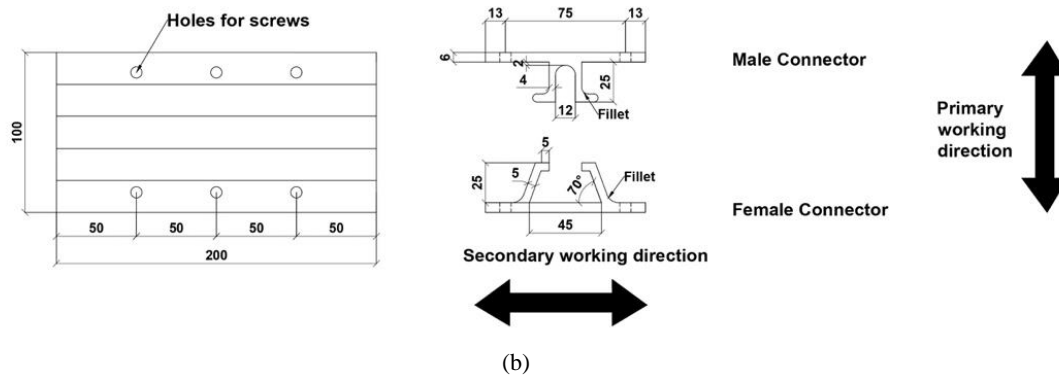


208 Fig. 6. The Illustrations of the working mechanism of the interlocking connection system (a) the modules assembly process
 209 with the interlocking connection system (b) the sectional elevation of the structure showing the overall constraints provided
 210 by the integrated interlocking connection system

211 **2.2 Description of the unit elements of the interlocking connectors**

212 Both tensile and shear connections have female connectors and male connectors, and each of them
 213 consists of repetitive unit patterns as demonstrated in Fig. 7. Their width is being determined according
 214 to the dimensions of conventional plate connections. The thickness of the bottom plate in all connectors
 215 was chosen based on the common practice of having steel plate thickness as $0.5d$ in double shear timber
 216 joints, to achieve adequate strength and avoid local deformation in the vicinity of screws [36]. The
 217 female connectors of both connections are groove-like devices, which are designed for accommodating
 218 the male connectors. The male connector in shear connection is formed by a cantilevering thin-walled
 219 curved steel band connected to a bottom steel plate via a cubic support at the middle, which is designed
 220 to deform during movement. In the unit element of the tensile male connector, two symmetric L-shaped
 221 steel components are connected to the steel plate with a 12mm gap in between for their free inward
 222 movement when sliding along the sloping walls of the female connector. The width of the gap was
 223 chosen corresponding to the maximum horizontal movement of the L-shaped components within the
 224 female connector before reaching the top. Both male connectors are designed to act as the damage
 225 control devices of the system and to yield first to isolate most of the deformation (without damaging
 226 other integral parts of the connections) before reaching the target displacement, so the female
 227 connectors, the timber and the fasteners can remain mostly intact (undeformed). In this way, the male
 228 connectors become the critical components that determine the strength and ductility in the interlocking
 229 connection, which ensure more predictable behaviours due to the less scattering properties of steel than
 230 timber. This can also contribute to a more reliable (finite element) simulation with only basic material
 231 properties such as compressive strength and tensile strength of timber and steel being used. Moreover,
 232 as the ductility in this interlocking connection is designed to be achieved in the steel connectors instead
 233 of the fasteners, large diameter screws ($\text{Ø}7\text{mm}$ - $\text{Ø}14\text{mm}$) are used in this connection system, which as
 234 suggested in the literature [8] [14] can improve load distribution and help to reduce the risk of in-service
 235 damage or brittle failure in timber. It is worth noting that in case of changing the damaged parts (units)
 236 of the connections, only the panels with the male connectors need removing.





237 Fig. 7. Schematic the basic units of interlocking connection (in mm): (a) shear connection (b) tensile connection

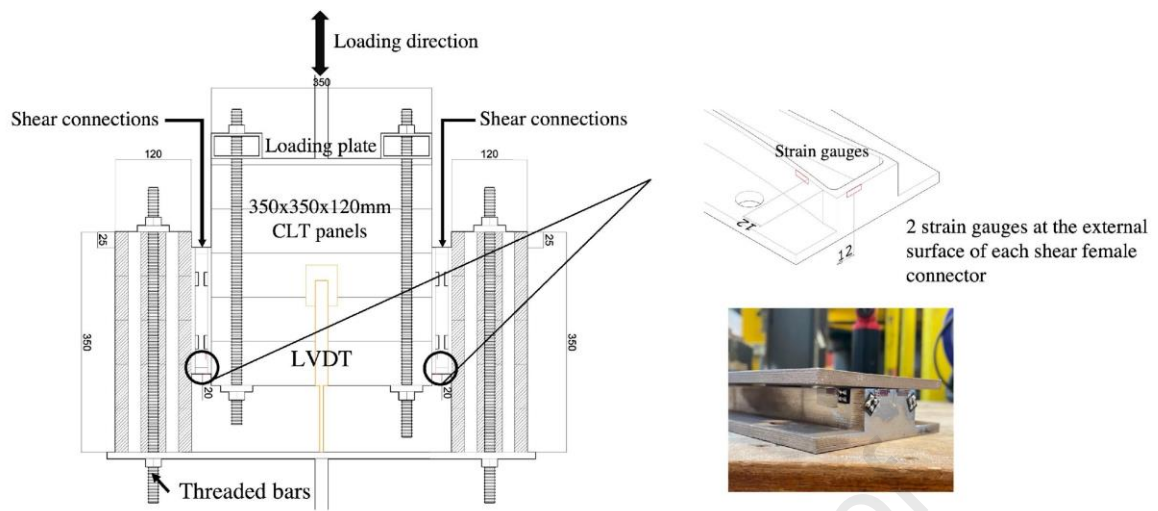
238 3. Experimental Testing

239 To assess the realistic performance of the proposed connection design and to develop reliable numerical
 240 models that can accurately simulate the connection performance, monotonic and cyclic tests were
 241 conducted on full-scale shear and tensile connection unit elements.

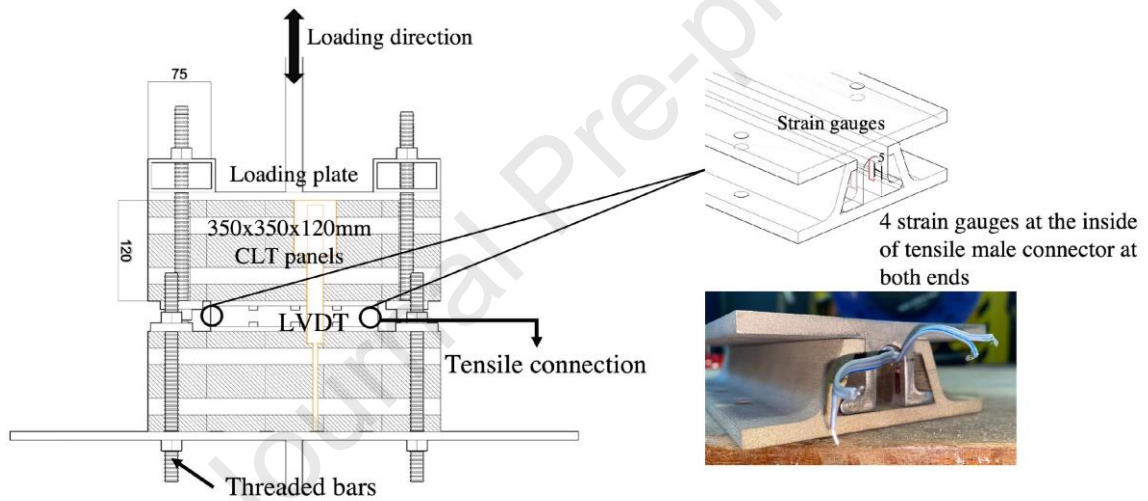
242 3.1 Test configuration and testing material preparation

243 Experimental set-ups for shear and tensile connections are shown in Fig. 8. To achieve symmetric test
 244 set-up for avoiding a moment being applied to the testing apparatus that may cause instability, two shear
 245 connections were tested together with three panels, while each tensile connection was tested
 246 individually. Overall, 3 monotonic tests (3 specimens) were conducted on the tensile connection and 1
 247 (2 specimens) on the shear connection under the rate of 0.05mm/s, and 2 cyclic tests (2 specimens) were
 248 performed on tensile connection and 1 (2 specimens) on shear connection under the speed of 0.02mm/s.
 249 In the quasi-static (cyclic) test, the loading protocol as prescribed in EN12512 [37] was adopted, with
 250 the estimated yield point V_{est} of 4mm for tensile connections and 2mm for shear connections according
 251 to the preliminary FE simulations. 4 strain gauges were attached to the specimens in each test with the
 252 locations of which being decided considering the preliminary numerical simulations and the
 253 accessibility of the assembled connections (Fig. 8).

254 All connection specimens were connected to 5-ply GL24h 350mmx350mmx120mm CLT panels with
 255 density varied between 435-470kg/m³ provided by Stora Enso using LBS7100 for the tensile
 256 connections and HBSP12120 for the shear connections. The locations of specimens on timber panels
 257 were all marked before the testing to measure the relative movement between timber and the steel
 258 connector. After being screwed to CLT panels, connection specimens were assembled by stacking
 259 (shear connection) or sliding (tensile connection) to form the experimental set-up and were tested
 260 without additional reinforcement. Mechanical and geometric properties of panels and screws are listed
 261 in Table 2 and Table 3. All CLT panels were conditioned in a controlled environment of 20°C with 65%
 262 humidity for the week before testing in accordance with EN 1380 [38], and all achieved the moisture
 263 content of 10%-10.8%, which were within the required range in the standard (10%-14%).



(a)



(b)



(c)



(d)

264

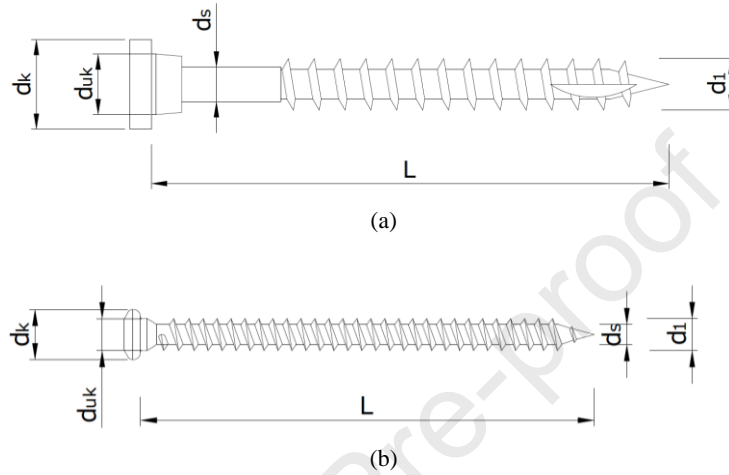
Fig. 8. Experimental set-up for (a)&(c) shear connection and (b)&(d) tensile connection

265

Table 2. Material properties for CLT panels (spruce) [39]

Elastic modulus (MPa)			Poisson's ratio			Shear modulus (MPa)		
E_{11}	E_{22}	E_{33}	ν_{12}	ν_{13}	ν_{23}	G_{12}	G_{13}	G_{23}
11000	370	370	0.48	0.48	0.22	690	690	50
Parallel-to-grain (MPa)		Perpendicular-to-grain (MPa)		Shear strength (MPa)				
f_{c11}	f_{t11}	f_{c22}	f_{t22}	f_v	$f_{v,roll}$			
36	24	4.3	0.7	6.9	0.5			

266



267

Fig. 9. Dimensions of screws: (a) HBSP12120 (b) LBS7100

268

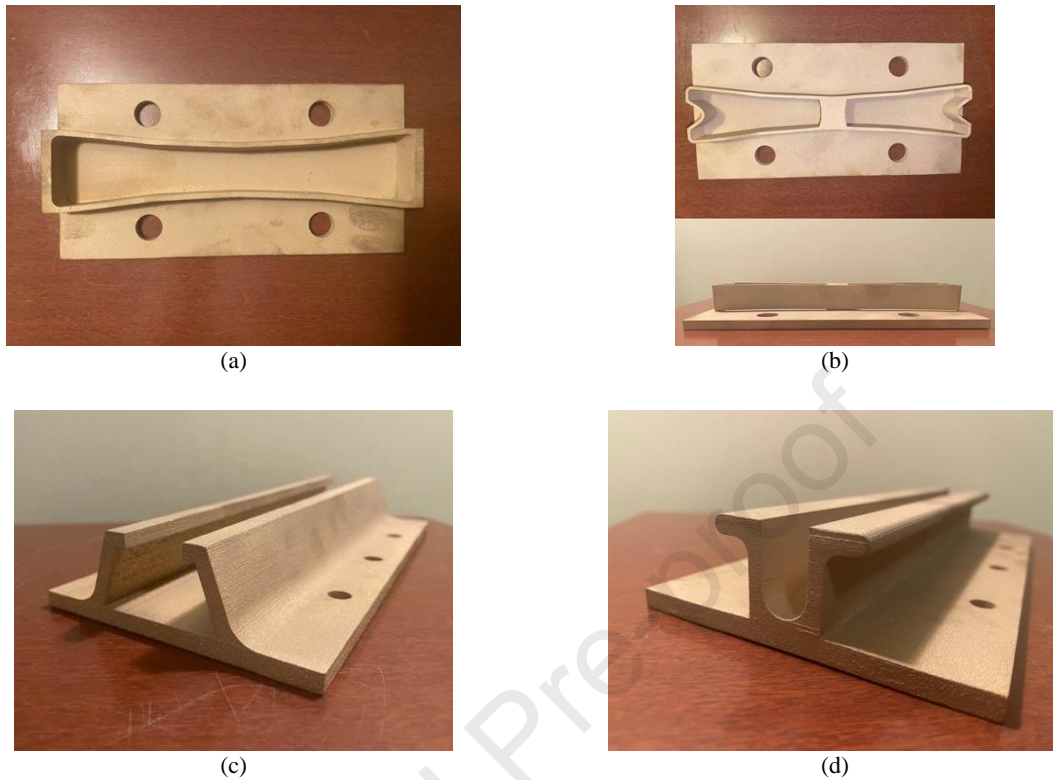
Table 3. Dimensions of screws used in experiment (in mm)

	L	d_1	d_s	d_k	d_{uk}
HBSP12120	120	12	8	20.75	14
LBS7100	100	7	4.4	11	7

269

270 The proposed novel connection specimens were 3D printed. Additive manufacturing was selected for
 271 its limitless fabrication capabilities, considering the new complex geometry with inclined and curved
 272 surfaces and the cantilevered steel band (Fig. 10(b)&(d)) of the proposed optimised connection designs.
 273 For the size of the proposed connections (Fig. 7), a metallic alloy composed of 60% 420 Stainless Steel
 274 as base material and 40% Bronze for additional strength and resistance was chosen in the printing with
 275 layer thickness of $100\mu\text{m}$ using Binder Jetting in Sculpteo [40]. The connection specimens were printed
 276 along the length of connection. This printing direction was chosen to achieve the most stable printing
 277 process and minimise the potential deformations in the cantilevering parts. Surface polishing was not
 278 an option for this size of specimens from the manufacturer, thus the 3D printed connections were all
 279 finished with granular surface (Fig. 10). To eliminate the risk of unpredictable behaviour due to the
 280 variation of friction during the movement of male connections within the female connections, the
 281 contact surfaces were polished to obtain smooth surfaces before testing. Despite the high manufacturing
 282 accuracy of 3D printing, 1mm tolerance was introduced in the printing of all connection specimens, to
 283 avoid the potential fitting issues caused by the dimensional distortion, considering the cantilevered
 284 feature and the scale of printing in this project. In the testing of tensile connections, the remaining gap
 285 after assembly was eliminated using the built-in function in the loading machine, while it is not
 286 achievable in the cyclic testing on the shear connections due to the reserve loading. Therefore, small

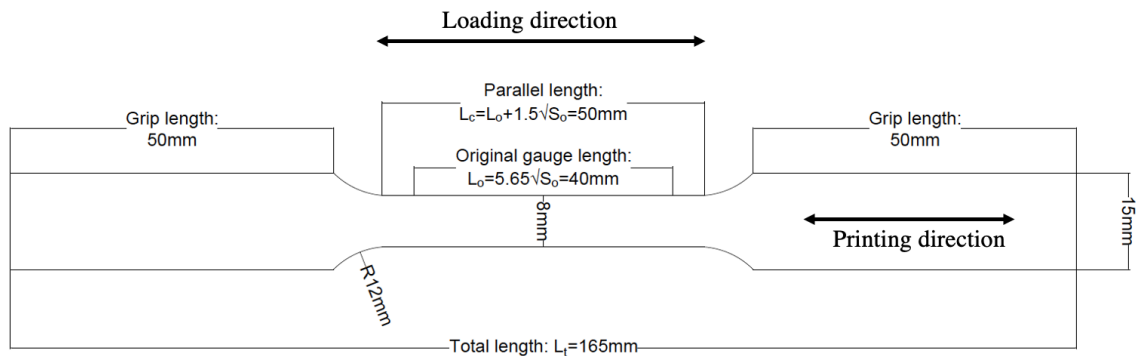
287 amount of sliding with no reaction force can be observed at the beginning of each loading step in the
 288 cycling testing on the shear connections.



289 Fig. 10. 3D printed connection specimens: (a) shear female connector; (b) shear male connector; (c) tensile female
 290 connector; (d) tensile male connector

291 3.2 Coupon test of 3D printed steel material

292 After the test, tensile coupon tests were undertaken to determine the tensile engineering stress-strain
 293 properties of the 3D printed SS420/BR in accordance with EN ISO 6892-1 [41] and support future
 294 numerical validation. Four coupons were machined from the bottom plates of the tested tensile female
 295 connectors (Fig. 12(a)), which experienced insignificant deformation during the testing. All specimens
 296 were tested in the direction that parallel to the printing direction under a constant speed of 3 mm/min
 297 using an Instron testing machine, with strain being measured by an extensometer attached to the
 298 coupons' surface.



299

300

Fig. 11. Dimensions of the specimens according to EN ISO 6892-1 [41]

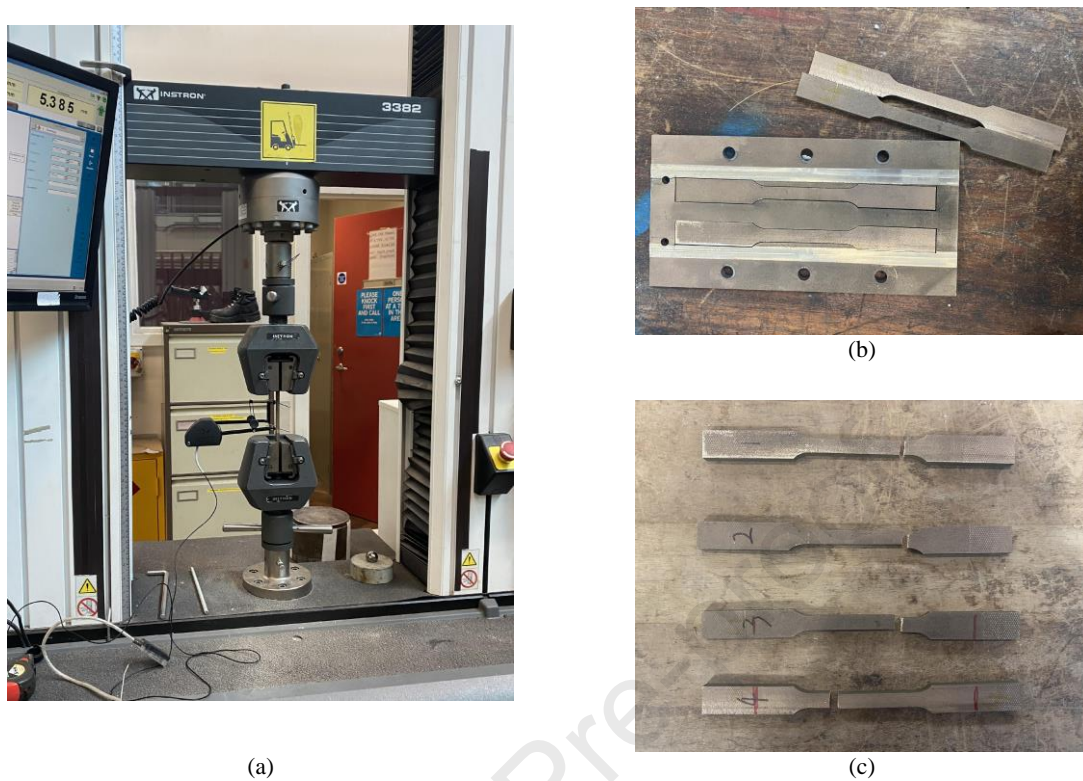
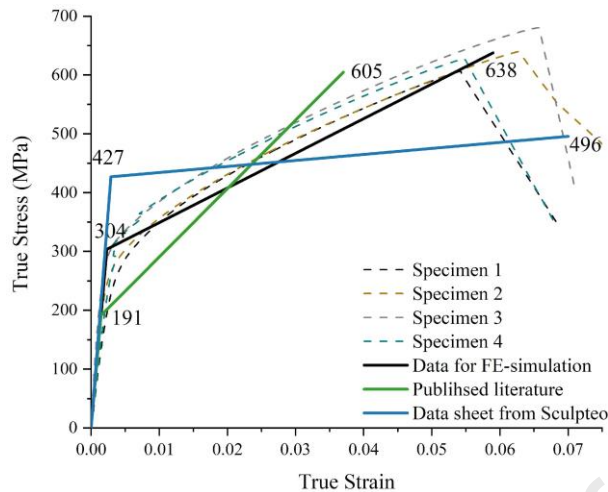
301
302

Fig. 12. Coupon test of SS420 (a) set-up for coupon test (b) machined coupons from the bottom plate of the tested tensile female connectors (c) specimens after testing

303
304
305
306
307
308
309
310
311
312
313
314
315
316
317
318

The original strain and stress data of the coupon tests were converted into true stress and strain, then the yield strength was calculated accordingly using 0.2% offset method. The generated data were relatively consistent with acceptable variation (Fig. 13), so the averaged properties from 4 coupon tests were adopted in the subsequent numerical study. In comparison with the material properties provided by the manufacturer [40] and the published coupon test data of SS420 [42] with the same printing layer thickness and printing direction, the adopted mean values for simulation have similar young's modulus and ultimate strain, while there are variations between the yield strength and the ultimate strength. These can attribute to the sensitivity of 3D printing material to the varied printing parameters such as travel speed and sintering temperature from different manufacturers. It should be noted that, 3D printed material has different behaviours in the directions perpendicular to and parallel to the printing direction. But the variations are only around 2-4% in two printing directions. According to the published experimental data [42], for the same 3D printed material in this research with the same printing layer thickness, the biggest property difference between directions parallel to and perpendicular to the printing direction is 2.1% in the ultimate strength. It can therefore conclude that, this difference would not affect the results significantly, and the material properties obtained in the printing direction of coupon specimen can well represent the material performance on different directions.



319

320

Fig. 13. Experimental data of coupon test and the mean material properties used as input data in simulation

321 4. Numerical Validation Model

322 To validate the numerical models using the experiment output, 3D fully-discretised continuum models
 323 of the tensile and shear connections with full details in the unit steel connectors, fasteners and timber
 324 were constructed in finite element analysis (FEA) software ABAQUS. Validated modelling methods in
 325 publications [43, 44] and nominal or tested material properties was employed in the validation models,
 326 which were analysed with ABAQUS/Standard. The dimensions of both connection specimens and the
 327 testing set-ups were set to be consistent with the test, as illustrated in Fig. 7, Fig. 8. and Fig. 9.

328 4.1 Modelling methods

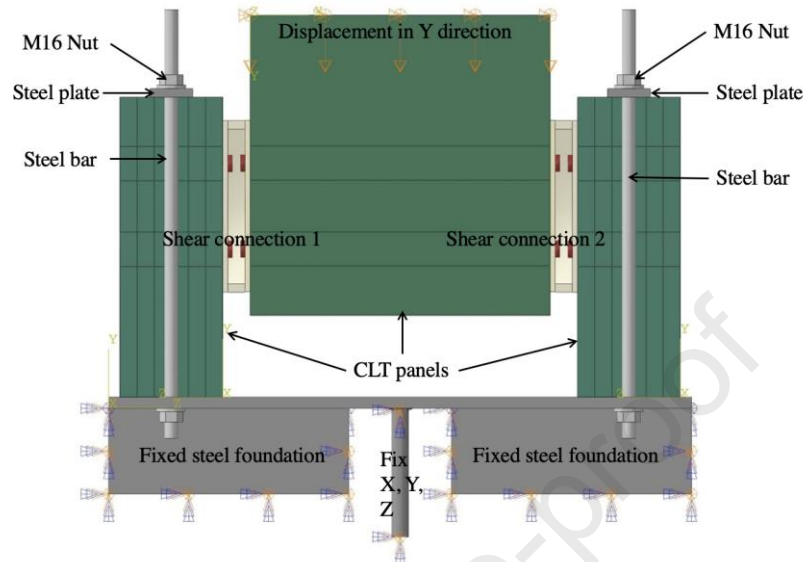
329 4.1.1 Materials

330 In the models of both tensile and shear connections, the 5-ply CLT panels were modelled using an
 331 orthotropic elastoplastic material model with the properties as listed in Table 2. Each layer of panel was
 332 considered separately with the first (20mm), third (40mm), and fifth (20mm) layers being loaded
 333 parallel to grain and the second (20mm) and fourth (20mm) layers being loaded perpendicular to grain.
 334 For all steel fixtures and screws, a modulus of elasticity 200GPa and a Poisson's ratio of 0.3 were
 335 assumed. Grade-300PLUS steel with a yield strength of 320MPa and an ultimate strength of 440MPa
 336 was used in all steel fixture devices. The Grade 10.9 carbon steel with a yield strength of 940.3MPa and
 337 an ultimate strength of 940.3MPa at 0.5% ultimate strain, was adopted for HBSP12120 and LBS7100,
 338 which were validated by Tomasi et al. [45]. For the modelling of the 3D printed connectors, a modulus
 339 of elasticity of 130GPa, a yield strength of 304MPa, an ultimate strength of 638MPa and an ultimate
 340 strain of 5.9 % that extracted from the coupon test were taken. 8-node linear brick with reduced
 341 integration (C3D8R) elements were adopted in the mesh throughout the model.

342 4.1.2 Modelling of shear connection

343 To better simulate the experiment with sufficient accuracy, the FE model of the shear connection was
 344 built according to the experiment set-up (Fig. 14(a)) with full dimensional details of steel fixtures as
 345 shown in Fig.8(a) and connections as shown in Fig.7(a) on both sides. The movement restrictions in
 346 three directions were applied on the steel foundations representing the support from the loading

347 machine, and on the grip bar connecting the entire test set-up to the loading machine. The middle panel
 348 with two shear male connectors attached was loaded in a displacement-controlled manner on top in Y-
 349 direction, simulating the load applied in the experiment.

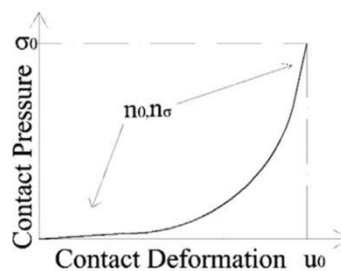


350

351

Fig. 14. The outline and boundary conditions of FE model of the shear connection

352 In the models of timber connections, the interfaces between timber and steel fasteners are crucial to the
 353 overall accuracy of the simulation. When loaded in shear, the screws in timber connections are mainly
 354 subjected to compression from the surrounding timber and the steel plate, which is mainly bored by the
 355 shank part of screws. Consequently, the screws in interlocking shear connection were modelled as
 356 cylindrical elements with a diameter equals to d_s in Table 3. The surface-to-surface discretisation
 357 method was adopted for the contact of all interfaces in the model with the “Hard Contact” option in the
 358 normal direction, and the “penalty friction formulation” option in the tangential direction, while using
 359 a coefficient of friction of 0.4 for all steel-steel contacts [43] and 0.25 for all steel-CLT contacts [46].
 360 Tie constraints were adopted in all interfaces between nuts and threaded bars to simulate the fastening
 361 effect, as no relative movements was observed during the test. In the tangential direction of the screws-
 362 timber interfaces, a non-linear relation of contact pressure and displacement (Eq.2) was used in the
 363 normal direction along with the “Tabular” option in ABAQUS to simulate the weakening effect of pre-
 364 drilling on the timber around screws, considering the chunky screws used in the shear connections.



365

366

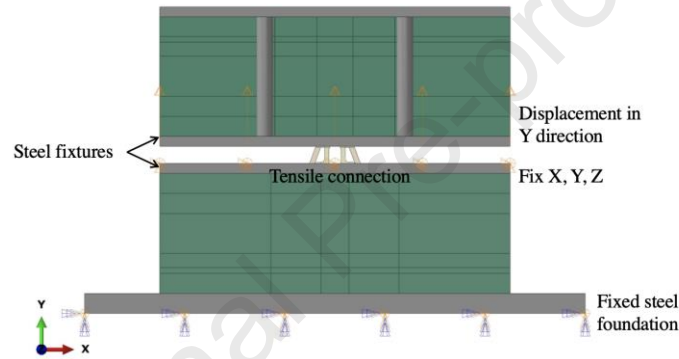
Fig. 15. Function represents the weakened timber around fasteners [43]

$$367 \quad \left(\frac{u_{inter}}{u_0}\right)n_u + \left(\frac{\sigma_0 - \sigma_L}{\sigma_0}\right)n_\sigma = 1 \quad (2)$$

368 Where n_u and n_σ are the control factors of the function curvature and were taken as 3.9 and 1.1, the
 369 contact deformation u_0 was taken as 0.35mm, all of which were extracted from the test on $\varnothing 12$ dowels
 370 conducted by Dorn [47]. σ_0 is the maximum compressive strength of timber that was assumed to be
 371 30MPa [43]. This formula represents the low timber strength around the surface of screws. Once the
 372 deformed screws reach the unaffected area, the strength of timber will be recovered.

373 4.1.3 Modelling of tensile connection

374 Similar to the shear connection model, the boundary conditions in the tensile connection model were
 375 set according to the experiment set-up. A simplified steel fixture was modelled for applying the
 376 movement restrictions as shown in Fig. 16. Displacement-controlled loading in the Y-direction was
 377 applied on the steel fixture on the panel with the male connector.



378 Fig. 16. The outline and boundary conditions of FE model of the tensile connection

379 When simulating timber screwed connections loaded in tension, two modelling methods are commonly
 380 adopted. The first one is to build the complete model of the screws including full details of the threaded
 381 part [48], thus the performance of screws is fully dependent on the geometric characteristics of screws
 382 and no assumption of screw properties is needed. The second one is a simplified method proposed and
 383 validated by Avez et al. [44] and Bedon et al. [49], which introduces a fictitious ‘soft material’ (Fig.
 384 17) to represent the threaded part with the diameter equals to d_1 in Table 3. The ‘soft material’ is
 385 assumed to be perfectly elastic and has the same capacity as the wood, except for the radial modulus
 386 that is reduced to 50MPa to eliminate its contribution in the compressive direction, representing the
 387 weakening effect of threads on the timber. Wrapped by ‘soft material’ is the ‘core’ that simulates the
 388 shank of screws, the dimensional value of which is taken as d_s of LBS7100 (Table 3). Compared to the
 389 first method, the second method is more computationally efficient due to the elimination of the small
 390 details of the threads and the large contacts area between the threads and timber, thus it is adopted in
 391 this study.

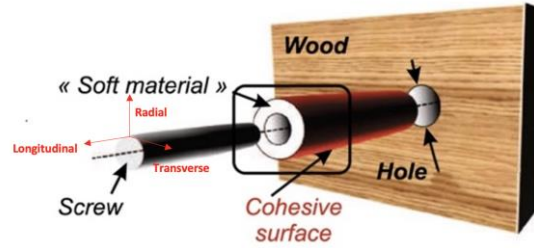


Fig. 17. Simplified FE model for screws in tension [38]

392

393

394 The withdrawal capacity of screws was simulated by a cohesive surface between the internal surface of
 395 drilled holes in the timber panel and the external surface of the ‘soft material’ with an assumed rigidity
 396 of 40N/mm^3 in the longitudinal direction and 0N/mm^3 in the tangential and radial directions (Fig. 17)
 397 [38]. The maximum nominal stress (MAXS) approach was applied at the cohesive surface in the
 398 ‘damage initiation criterion’ option to simulate the initiation of interaction failure:

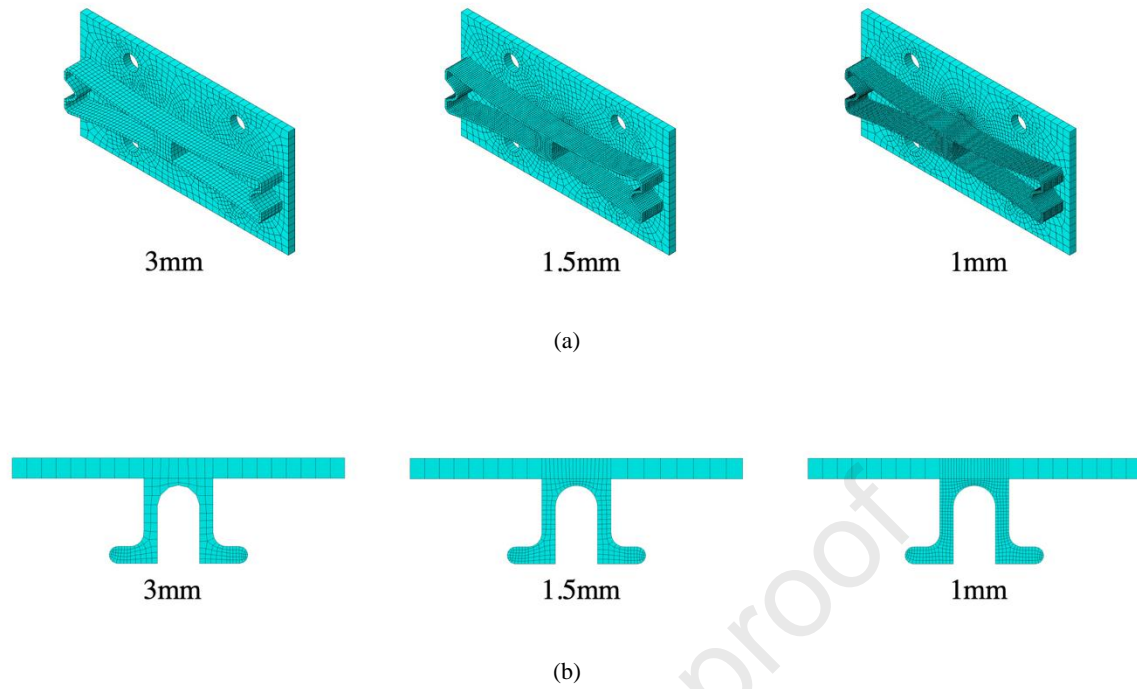
$$399 \quad \max\left\{\frac{t_n}{t_n^0}, \frac{t_s}{t_s^0}, \frac{t_t}{t_t^0}\right\} = 1 \quad (3)$$

400 where the t_n^0 , t_s^0 and t_t^0 are the peak allowable stresses in the normal (n), first (s) and second (t)
 401 direction of the bonding interface, the values of which were taken as 36MPa, 6.9MPa and 6.9MPa,
 402 equalling to the compressive and shear strength of timber as listed in Table 2.

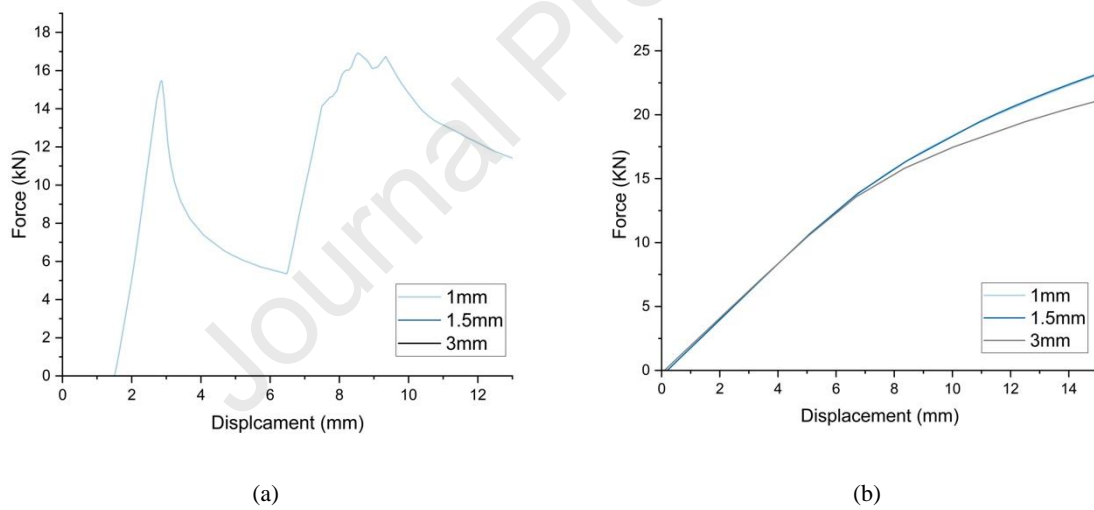
403 After the cohesive resistance is reached, the strength degradation of bonding begins and the brittle post-
 404 damage behaviour of the connection under tension interaction was simulated by a ‘linear damage
 405 evolution’ law, assuming that the full residual stiffness of the cohesive surface is achieved when 4mm
 406 deformation first attained, so the contact behaviour became elastic-brittle, simulating the brittle failure
 407 of dowel-type timber connection under tension. The cohesive interaction was combined with “Hard
 408 Contact” in the normal direction and the “Penalty Friction Formulation” with a coefficient of friction
 409 of 0.4 in the tangential direction to avoid the penetration of screws into timber at the post-failure stage.

410 4.1.4 Mesh sensitivity

411 To study the impact of mesh size on the FE predictions and ensure the adequate adoption of mesh size,
 412 the mesh sensitivity analysis was conducted. The timber panels, fasteners, metal fixtures and the female
 413 connectors, which experienced insignificantly deformation in the test, were proved to be independent
 414 to the mesh size. Therefore, increasingly smaller mesh size was only applied in the interested areas of
 415 both connection models (Fig.18), while the mesh size in other parts of the testing set-up remained
 416 consistent. The male connectors of both connections, which are designed to govern connection
 417 properties, were first studied with 3mm mesh size. Then the mesh size was refined to 1.5mm and 1mm.
 418 It can be observed in Fig.19(a) that, the changes in mesh size have little impacts on the numerical
 419 predictions of shear connector model. In the model of tensile male connector (Fig.19(b)), the initial
 420 stiffness is independent to the mesh size, while yielding strength is slightly sensitive. The 1.5 mm mesh
 421 size showed a good compromise between results accuracy and the calculation efficiency in both models.
 422 It was therefore chosen in the subsequent study.



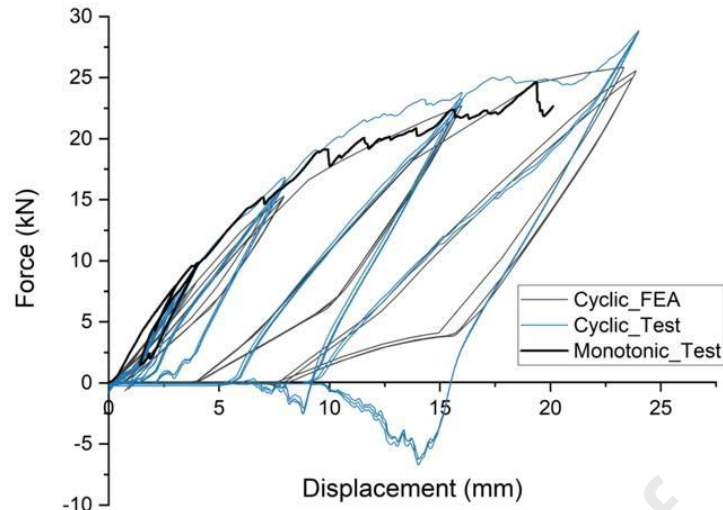
423 Fig. 18. Mesh size considered in the mesh sensitivity study of (a) shear male connector (b) tensile male connector



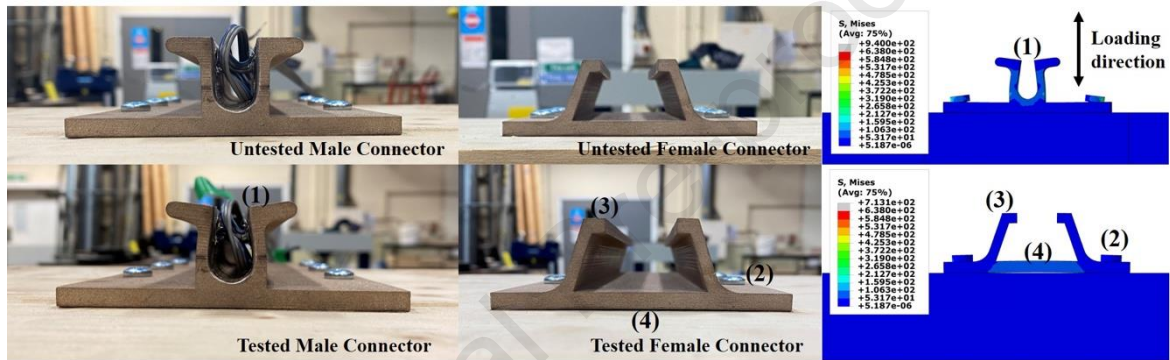
424 Fig. 19. Force-displacement response obtained from different mesh size in (a) shear male connector model and (b) tensile male
425 connector model

426 4.2 Numerical Validation

427 4.2.1 Tensile connection



(a)



(b)

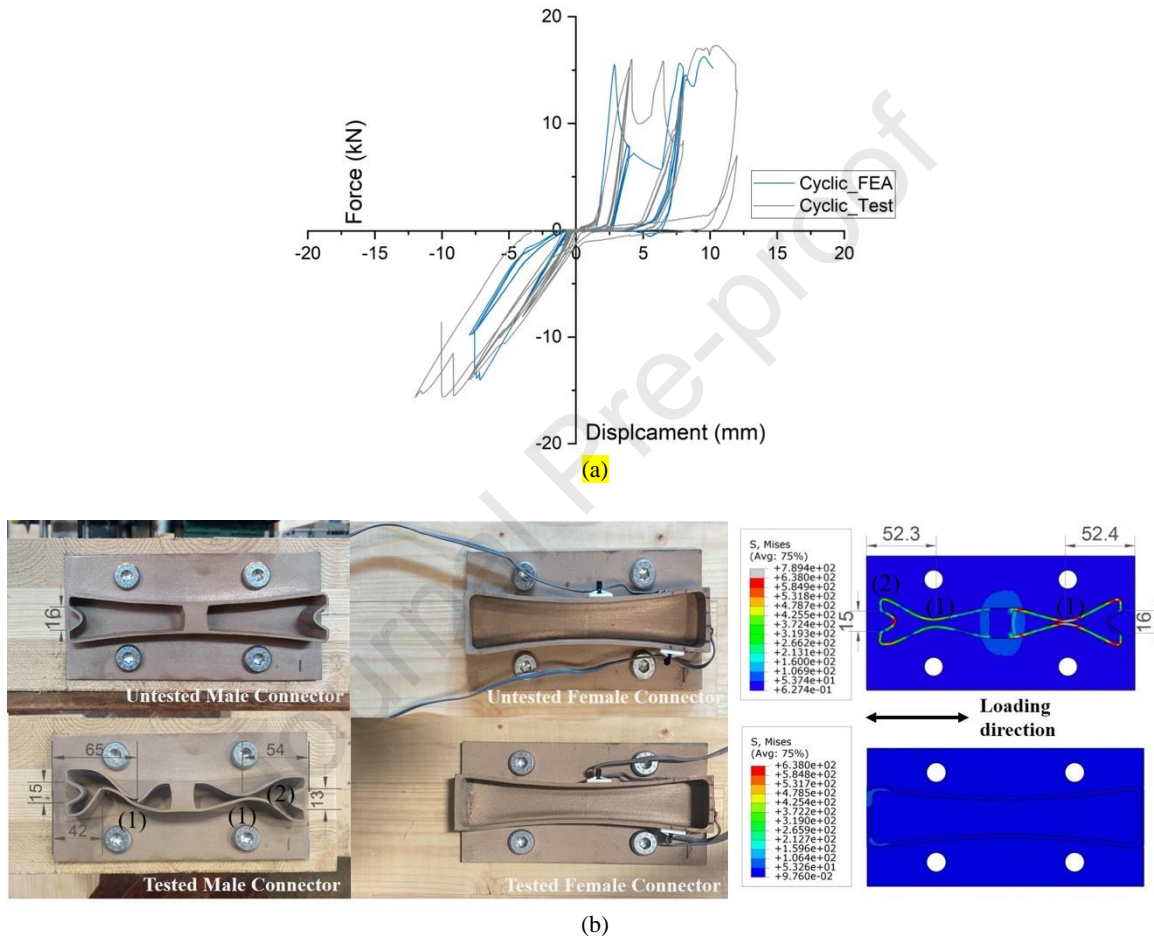
428 Fig. 20. Comparisons between experimental result and FEA in (a) hysteresis loops and (b) the deformation modes in tensile
 429 connection specimens (in mm)

430 Fig. 20(a) shows the hysteresis loops for the proposed tensile connections. Different from conventional
 431 timber connections, the connection performance in the first cycle of each loading step in cyclic test
 432 showed good consistency with the monotonic test, as stiffness and maximum strength in monotonic
 433 loading at each step can be reached in cyclic loading with no strength degradation, indicating the plastic
 434 deformation in the steel male connector does not affect the maximum capacity in the subsequent
 435 loading. However, the plastic deformation caused gaps between two connectors, leading to the sliding
 436 of the male connector within the female connector with no reaction force. With the increase in applied
 437 displacement, the bearing walls of the female connector started to open-up and close elastically, along
 438 with the upward and downward movement of the male connector. This indicated that the bearing walls
 439 also contributed to the connection stiffness under large displacement, which led to the degraded stiffness
 440 degradation of each repeated circle, as similar to the pinching effect in the conventional timber
 441 connections.

442 The primary deformation mode in the tensile connection was the bending of the L-shaped elements in
 443 the male connector as designed (point 1 in Fig. 20(b)). The female connector and screws on the other
 444 hand, remained mostly undeformed (point 2 in Fig. 20(b)), and only very slight open-up in the bearing
 445 walls (point 3 in Fig. 20(b)) and slight bending in the bottom plate (point 4 in Fig. 20(b)) were visible
 446 at the end of testing, so the deformed male connector can be easily slide out.

447 The FE model of tensile connection has good agreement with the experimental output, as the maximum
 448 strength of each loading cycle, the initial and reduced stiffness can all be well captured. Four
 449 deformation modes in the tensile connection as discussed above were also well reproduced in terms of
 450 shape and dimension, proving the feasibility of the proposed modelling method for interlocking tensile
 451 connection. Though slight pulling out can be observed from the screws in male connector in the model,
 452 the continuous force-displacement curve indicated that the screws-timber interfaces still remained
 453 elastic, as the ‘linear damage evolution’ in FE model was not activated.

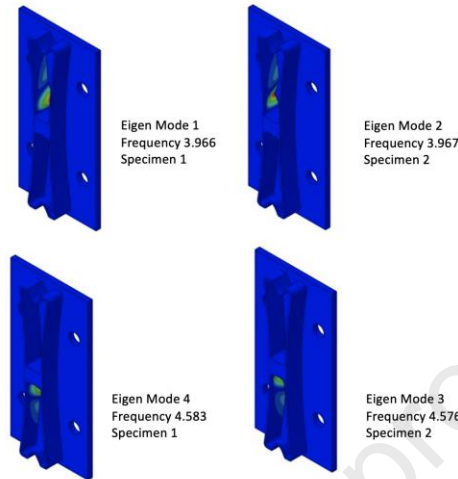
454 4.2.2 Shear connection



455 Fig. 21. Comparisons between experimental result and FEA in (a) hysteresis loops and (b) the deformation modes in shear
 456 connection specimens at -8mm displacement (in:mm)

457 In the cyclic testing of shear connections (Fig. 21(a)), a sudden drop in force can be observed when first
 458 reaching the displacement of 4mm, which was followed by another one at the displacement of 6.5mm
 459 under the similar forces (around 16kN). These indicated the buckling happened in the shear connections
 460 on both sides (point 1 in Fig. 21(b)), which caused instability in the experimental set-up. After the
 461 buckling, the connection strength continued to develop in the deformed steel band and the end sunken
 462 (point 2 in Fig. 21(b)), until the breakage happened at the buckling point of one shear connection (Fig.
 463 21(b)), leading to the plumper hysteresis loop at large displacement. Therefore, two major deformation
 464 modes can be identified in the tested shear connections after the testing: buckling at the middle of the
 465 deformable band and bending at the sunken design at the end of the steel band. As shown in Fig. 21(a),
 466 the buckling and plastic deformations in the shear connection specimens caused unsymmetric

467 behaviours in two loading directions, which are unfavourable considering the stability of structures and
 468 limit the connection's capacity in dissipating energy. The buckling locations were relatively consistent
 469 among all the specimens, while unsymmetric buckling shapes can be observed in some specimens due
 470 to manufacturing imperfections and the post-buckling loading on the buckled steel elements.



471

472

Fig. 22. Four Buckling Modes Extracted by 'Block Lanczos' Method

473 As buckling was observed in the shear connection, geometrically and materially nonlinear analysis with
 474 imperfections included (GMNIA) was conducted in the shear connection validation model. The linear
 475 Eigen-buckling analysis, which is a common method for predicting the buckling strength and generating
 476 'imperfection' on the model to trigger nonlinear buckling analysis, was first conducted. In the Eigen
 477 buckling analysis, a unit pressure was applied at the mid-span to predict the critical load of buckling
 478 and the buckling mode shapes of the ideal structure based on the 'Block Lanczos' method. As shown
 479 in Fig. 22, the generated four buckling modes in the male connectors on both sides agreed qualitatively
 480 with the test results, so they were extracted and imported into the nonlinear analysis as 'imperfection'
 481 with a factor of 0.2. As the primary deformation form in the tensile male connector was bending instead
 482 of buckling, GMNIA was not considered in the tensile connector model.

483 With the inclusion of 1mm gap in the shear connection model, sliding in the initial stage of each loading
 484 step that corresponding to the experiment can be observed in the numerical output. The model with the
 485 initial imperfections was able to simulate the negative stiffness of buckling. The buckling shapes on
 486 both sides as well as the bending at the end sunken were also well reproduced in terms of locations and
 487 dimensions, which proves the adequate accuracy of the validation model.

488 4.3 Conclusions

489 The results of the monotonic and cyclic tests on the shear and tensile connections demonstrated that,
 490 two connections behaved very differently in terms of mechanical properties and deformation forms.
 491 The tensile connection had lower stiffness but higher maximum strength and better ductility with a
 492 ductile failure mode (due to bending), while the shear connection showed higher stiffness but lower
 493 maximum strength and ductility with a brittle failure mode (due to buckling). In both connections, there
 494 was no sign of pulling out in screws and no visible relative movement between the connectors and
 495 timber (Fig. 23) after the attainment of the maximum strength. These indicated that the deformation
 496 was successfully managed within the male connectors in both shear and tensile connections, with very
 497 small deformation developed in the female connector but without any brittle breakage in timber. This
 498 is a clear demonstration of the ability of connections to localise plastic deformation within the male
 499 connectors under the control damage approach.



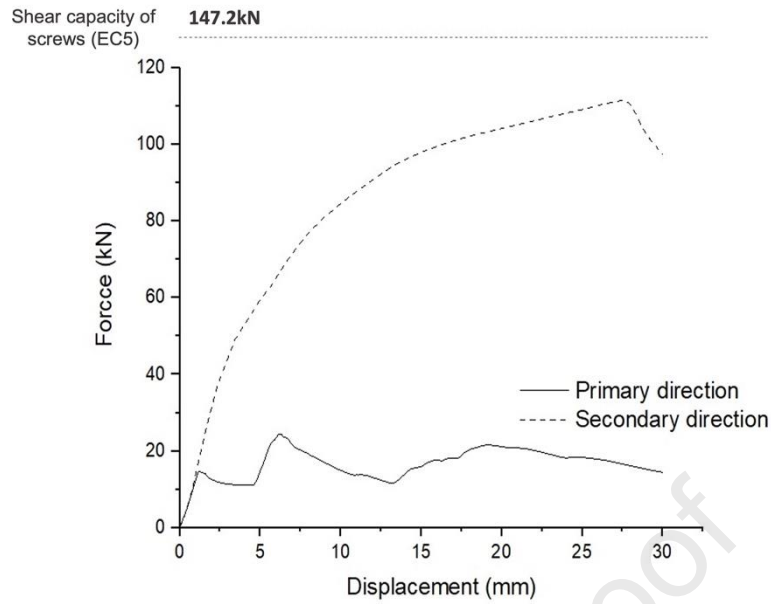
Fig. 23. Removal of screws from (a) shear connections and (b) tensile connection after test

501 5. Numerical Simulations

502 To further characterise the translational behaviours of the proposed shear and tensile connections and
 503 explore their potential with more common and ductile steel material (S235), a monotonic analysis was
 504 performed in the validated models at the primary and the secondary working directions (Fig. 7) of both
 505 connections, with material properties of S235 (modulus of elasticity of 210GPa, yield strength of
 506 235MPa and ultimate strength of 360MPa).

507 5.1 Translational behaviours of the shear connection

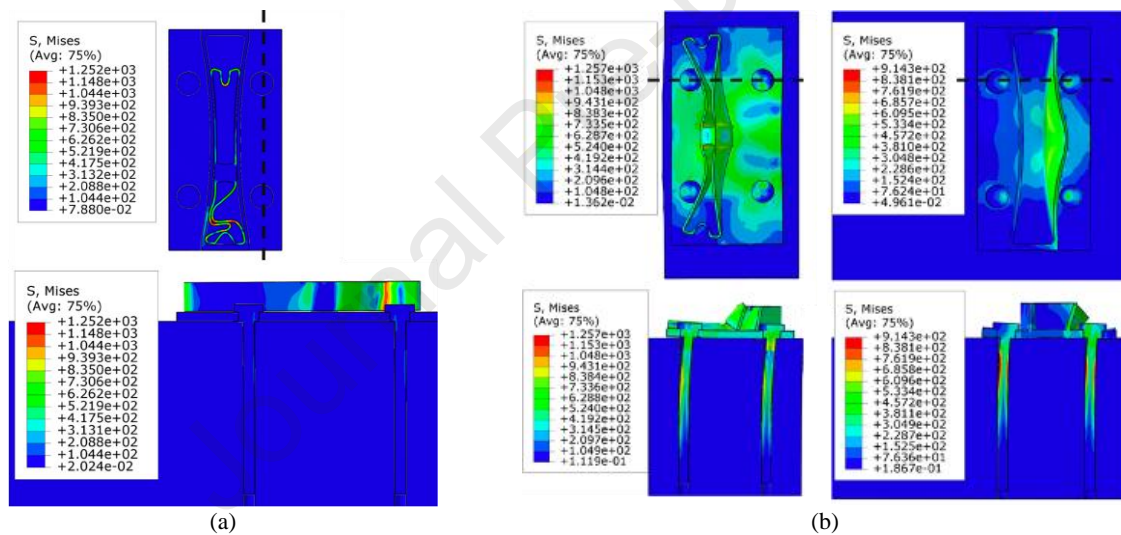
508 The force-displacement responses of the interlocking shear connection FE model in the primary and
 509 secondary directions are reported in Fig. 22. The numerical model can also monitor the deformation
 510 developing trends in the shear connections to help better understand the connection behaviours, which
 511 was not available in the test due to the concealed design nature of the shear connection. Similar to the
 512 tested specimens, the shear connection with S235 first buckled at the cantilevered steel band, resulting
 513 in negative stiffness in the FE model. With the continuous loading, the buckled steel band continued to
 514 bend and the deformation started to develop in the end sucken on the other side. Corresponding to the
 515 experiments, most of the plasticity was observed in the designated deformable band (Fig. 25(a)) in the
 516 male connector after a 30mm displacement in the primary direction, while litter plastic strain was
 517 developed in the female connector and fasteners, which also resulted in very small damage on timber
 518 panels.



519

520

Fig. 24. Force and displacement curve of interlocking shear connection



521

522

Fig. 25. Stress distribution on shear connections and screws under the displacement of 30mm in (a) the primary direction and (b) the secondary direction

523

524

525

526

527

When working in the secondary direction, the interlocking shear connection showed much higher strength and ductility than that in the primary direction, but the process of plastic deformation was mainly managed by the bending of the middle cubic support in the male connector and the bending of the wall in the female connector at the loaded side. The increased plastic strain in the screws proved that the fasteners also contributed to the connection strength when working in the secondary direction.

528

5.2 Translational behaviours of the tensile connection

529

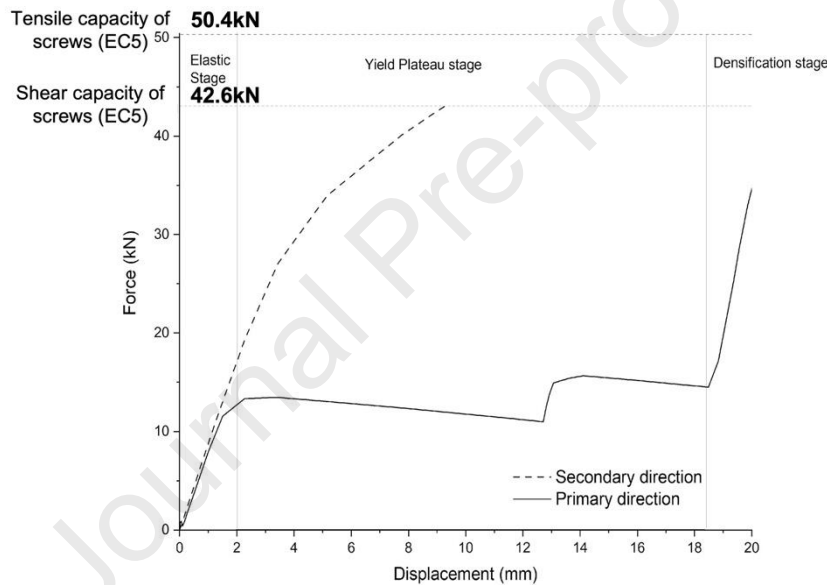
530

531

532

As demonstrated in Fig. 24, the behaviour of the interlocking tensile connection with S235 in the primary working direction can be classified into three stages: the elastic stage, the yield plateau stage, and the densification stage. When the loading started, the male connector started to move upwards within the female connector, and the sloping walls of which compressed the L-shaped elements to bend

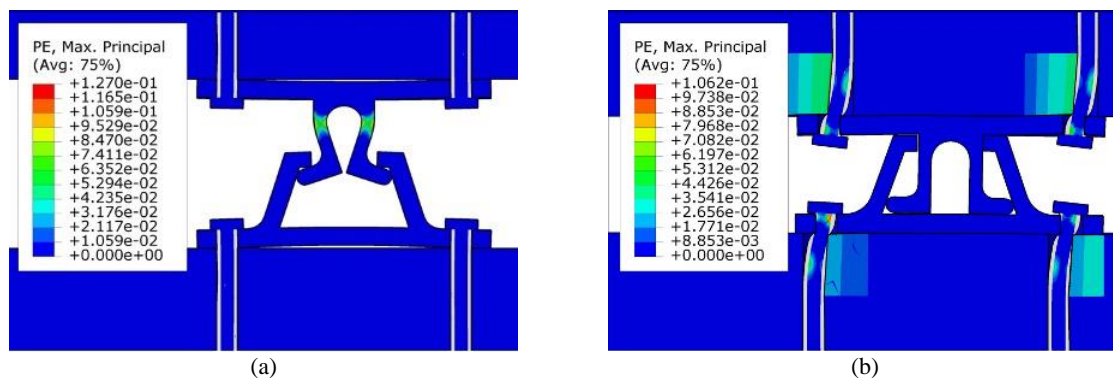
533 inwards. With the continuous vertical movement of the male connector, the L-shaped elements yielded
 534 and the walls of the female connector started to open up slowly due to the increased moment at the wall
 535 base, resulting in slightly decreased reaction force of the connection at the yield plateau stage. When
 536 the male connector came into contact with the top of the female connector, it stopped moving and the
 537 stiffness of the connection increased significantly, indicating that the behaviour of connection enters
 538 the densification stage, in which the connection becomes rigid to prevent further displacement
 539 (opening). Thus, the $F-\delta$ curve of tensile connection in the primary working direction can be idealised
 540 using three parameters: the initial stiffness, the yielding strength and the displacement at the onset of
 541 densification. Fig. 27 shows that, at the displacement of 15mm in the primary working direction, the L-
 542 shaped elements in the male connection processed most of the plastic deformation, while little can be
 543 observed in other connection components. Though the stress of the screws under tension cannot be
 544 reflected directly from the stress contour due to the employment of fictitious elastic 'soft material', no
 545 strength reduction can be observed in the force-displacement curve, indicating that brittle failure did
 546 not appear in screws at 20mm slip and the screws were still in the elastic stage.



547

548

Fig. 26. Force and displacement curve of interlocking tensile connection



549

550

Fig. 27. Von Mises Stress contour in the interlocking tensile connections under the displacement of 15mm in (a) the primary direction and (b) the secondary direction

551 When loaded in the secondary working direction, the plastic strain contour plot depicts that the
552 interlocking tensile connection developed a similar working mechanism to the conventional steel plate
553 connections, in which the bending of screws and the crushing of timber are the primary deformation
554 modes. The embedment strength of timber and the bending strength of screws therefore became the
555 main contributors of the connection strength, while the interlocking steel connectors were relatively
556 rigid.

557 **6. Discussions and Limitations**

558 The FE models of both interlocking shear and tensile connections with S235 demonstrated that the
559 proposed connection designs can provide adequate strength and ductility under translational forces.
560 When working in the primary direction, the male connectors in both connections yielded before
561 reaching the full capacity of the surrounding fasteners, so most of the plastic deformation is managed
562 within the designated areas (male connectors), while the female connectors, fasteners and timber remain
563 mostly intact. This indicates that the dissipating element in the novel interlocking connection shifts
564 from the fasteners like in conventional connections to the steel elements in the new connection. With
565 the specially designed deformable steel elements, this connection system can absorb energy in
566 predictable manners, preventing plastic deformation from developing in fasteners and timber to avoid
567 brittle failure and reducing the risk of significant failure of structures under extraordinary loads such as
568 seismic load. In addition, the initial deformation of the steel male connectors can be monitored and act
569 as an early warning system since they can be relatively easy to access. This also means that only the
570 male connector would fail after a severe event and needs to be repaired or replaced, while the screws
571 connecting the unit and the panel will remain intact and thus the timber fibres will not be affected by
572 the bending of the screws as it is normally the case. It therefore helps to improve the structural integrity
573 and to reduce the time needed for maintenance. When damage happens in the connection units, the
574 damaged module can be removed following the installation sequence for the repair or replacement. Due
575 to the short unit length of connection (same to the steel specimen dimensions), rapid and cost-effective
576 supply can be achieved with 3D printing of the male connector. Also, the timber panels can be fully
577 reused since the proposed novel connection system promotes no fastener failure.

578 In the secondary working direction, the deformation in the connection is less ductile and managed by
579 the composite effect between the fasteners and the steel connector, which is similar to the working
580 mechanism of the conventional steel plate connections and is characterised by its high stiffness but
581 relative lower ductility than in the primary working direction. When comparing the deformation forms
582 in two working directions, the significantly reduced deformation in screws in the primary direction
583 indicates the successful damage control in connections through the introduction of the proposed
584 connector design.

585 Different from other novel connections for CLT volumetric structures, the one proposed in this study
586 requires no modifications for fitting, thus is applicable to different flat module specifications. The
587 equipped damage-limiting capacity also makes it superior to the conventional connection in terms of
588 life-safety performance and material reuse after the end-of-life of structures. The proposed connection
589 system holds the potential of improving the dismantlability in CLT volumetric structures, promoting a
590 more flexible volumetric construction with changeable, demountable and fully reusable structural
591 elements.

592 Despite the superiorities, the immediate practical application of the proposed connection system may
 593 be limited by the existing construction tools. The sliding and stacking of modules require specially-
 594 designed lifting and moving machines and scaffolds frames. Also, due to the geometric complexity, the
 595 mass production of the proposed connections is difficult to be achieved with the conventional
 596 manufacturing methods. However, with the gradually increasing manufacturing scale of 3D printing
 597 and the reducing printing cost, the mass production is expected to be achievable with 3D printing in the
 598 future.

599 **7. Conclusions**

600 In this paper, a comprehensive review of the recent advancements in the study of connection systems
 601 for CLT volumetric structures is first provided. The factors that relate to connection systems and
 602 constrain the development of multi-storey CLT volumetric structures have been analysed and
 603 summarised. As a result, a novel interlocking connection system is then proposed for addressing the
 604 low construction efficiency, inaccessibility of inter-module connections and the insufficient ductility of
 605 typical timber connections in VTC. The designed ability of managing deformations within one part of
 606 the connection and eliminating damage in timber panels in the primary working direction was proved
 607 via experiments and numerical analyses on the 3D printed connection specimens. Numerical models
 608 with good accuracy were proposed for both connections using only nominal material properties, owing
 609 to the fact that the load-carrying capacity and ductility are correlated to the proposed interlocking metal
 610 connectors. Ultimately, the adequate translational strength and ductility of the proposed connections
 611 were proved by the validated numerical models.

612 Future research will include a comprehensive parametric study to identify the critical parameters of the
 613 proposed connection systems and their detailed mechanical properties, as well as conduct a direct
 614 comparative study between typical connections and the novel connection system via global models of
 615 a full-scale CLT volumetric building. The study will be centred to the contribution of the connections
 616 to the overall lateral resistance of the structure.

617 **Acknowledgements**

618 The authors and the 3DMBC (<https://3dmbc.com>) group members would like to acknowledge the Royal
 619 Academy of Engineering and The Leverhulme Trust funds [LTSRF1819_15_40] as well as The Henry
 620 Lester Trust funds for their financial support in 3D printing the connection specimens. The contribution
 621 of The George Earle Laboratory staff is also acknowledged for providing technical expertise for the
 622 experimental testing. The authors would also like to recognise the support from Rothoblaas and Stora
 623 Enso on the testing materials (screws and CLT panels).

624 **References**

- 625 [1] Pan, M., Pan, W. *A comparison between Volumetric Timber Manufacturing Strategies in*
 626 *the UK and mainland Europe*. Modular and Offsite Construction (MOC) Summit Proceedings,
 627 2016.
 628 [2] Carvalho, L.F., Jorge, L.F.C. and Jerónimo, R. *Plug-and-Play Multistory Mass Timber*
 629 *Buildings: Achievements and Potentials*. Journal of Architectural Engineering, 2020. **26**(2).
 630 [3] Stepinac, M., Šušteršič, I., Gavrić, I., Rajčić, V. *Seismic Design of Timber Buildings:*
 631 *Highlighted Challenges and Future Trends*. Applied sciences, 2020. **10**(4): p. 1380.

- 632 [4] Fragiacomò, M., Dujic, B. and Sustersic, I. *Elastic and ductile design of multi-storey*
633 *crosslam massive wooden buildings under seismic actions*. Engineering Structures, 2011.
634 **33**(11): p. 3043-3053.
- 635 [5] Pozza, L., Scotta, R., Trutalli, D., Pinna, M., Polastri, A., Bertoni, P. *Experimental and*
636 *Numerical Analyses of New Massive Wooden Shear-Wall Systems*. Buildings (Basel), 2014.
637 **4**(3): p. 355-374.
- 638 [6] Sandhaas, C. and Ceccotti, A. *Earthquake resistance of multi-storey massive timber*
639 *buildings*. 2012. In; Forum Holzbau 12.
- 640 [7] Ceccotti, A., Sandhass, C., Okabe, M., Yasumura, M., Minowa, C., Kawai, N. *SOFIE*
641 *project - 3D shaking table test on a seven-storey full-scale cross-laminated timber building*.
642 Earthquake engineering & structural dynamics, 2013. **42**(13): p. 2003-2021.
- 643 [8] Gavric, I., Fragiacomò, M. and Ceccotti, A. *Cyclic behaviour of typical metal connectors*
644 *for cross-laminated (CLT) structures*. Materials and structures, 2015. **48**(6): p. 1841-1857.
- 645 [9] Li, Z., Tsavdaridis, K.D. and Gardner, L. *A Review of Optimised Additively Manufactured*
646 *Steel Connections for Modular Building Systems*. 2020: Springer International Publishing.
- 647 [10] Malo, K.A., Abrahamsen, R.B. and Bjertnæs, M.A. *Some structural design issues of the*
648 *14-storey timber framed building “Treet” in Norway*. European Journal of Wood and Wood
649 Products, 2016. **74**(3): p. 407-424.
- 650 [11] Stora Enso. *3–8 Storey Modular Element Buildings*. Available from:
651 [https://www.storaenso.com/-/media/documents/download-center/documents/product-](https://www.storaenso.com/-/media/documents/download-center/documents/product-brochures/wood-products/design-manual-a4-modular-element-buildings20161227finalversion-40en.pdf)
652 [brochures/wood-products/design-manual-a4-modular-element-](https://www.storaenso.com/-/media/documents/download-center/documents/product-brochures/wood-products/design-manual-a4-modular-element-buildings20161227finalversion-40en.pdf)
653 [buildings20161227finalversion-40en.pdf](https://www.storaenso.com/-/media/documents/download-center/documents/product-brochures/wood-products/design-manual-a4-modular-element-buildings20161227finalversion-40en.pdf).
- 654 [12] O’Ceallaigh, C. and Harte, A.M. *The elastic and ductile behaviour of CLT wall-floor*
655 *connections and the influence of fastener length*. Engineering Structures, 2019. **189**: p. 319-
656 331.
- 657 [13] EN 1998-1. *Eurocode 8-Design of structures for earthquake resistance - part 1: General*
658 *rules, seismic actions and rules for buildings*. European Committee for Standardisation, 2004.
- 659 [14] Chan, N., Hashemi, A., Zarnani, P., Quenneville, P. *Pinching-Free Connector for Timber*
660 *Structures*. Journal of Structural Engineering (New York, N.Y.), 2021. **147**(5): p. 4021036.
- 661 [15] Iacovidou, E. and Purnell, P. *Mining the physical infrastructure: Opportunities, barriers*
662 *and interventions in promoting structural components reuse*. The Science of the Total
663 Environment, 2016. **557-558**: p. 791-807.
- 664 [16] EN 1995-1-1. *Eurocode 5-Design of timber structures-part 1-1: General common rules*
665 *and rules for buildings*. European Committee for Standardisation, 2004.
- 666 [17] Trutalli, D., Marchi, L., Scotta, R., Pozza, L. *Capacity design of traditional and innovative*
667 *ductile connections for earthquake-resistant CLT structures*. Bulletin of Earthquake
668 Engineering, 2019. **17** (4): p. 2115-2136.
- 669 [18] Jorissen, A. and Fragiacomò, M. *General notes on ductility in timber structures*.
670 Engineering Structures, 2011. **33**(11): p. 2987-2997.
- 671 [19] Izzi, M., Casagrande, D., Bezzi, S., Pasca, D., Follesa, M., Tomasi, R. *Seismic behaviour*
672 *of Cross-Laminated Timber structures: A state-of-the-art review*. Engineering Structures,
673 2018. **170**: p. 42-52.
- 674 [20] Izzi, M., Polastri, A., and Fragiacomò, M. *Modelling the mechanical behaviour of typical*
675 *wall-to-floor connection systems for cross-laminated timber structures*. Engineering
676 Structures, 2018. **162**: p. 270-282.
- 677 [21] Sharafi P, Mortazavi M, Samali B, Ronagh H. *Interlocking system for enhancing the*
678 *integrity of multi-storey modular buildings*. Automation in construction, 2018. **85**: p. 263-272.
- 679 [22] Di Pasquale, J., Innella, F. and Bai, Y. *Structural Concept and Solution for Hybrid*
680 *Modular Buildings with Removable Modules*. Journal of Architectural Engineering, 2020.
681 **26**(3): p. 4020032.

- 682 [23] Gijzen, R. *Modular cross-laminated timber buildings*, in the faculty of Civil Engineering
683 *and Geosciences*. 2017, Delft University of Technology.
- 684 [24] Zhang, C., Lee, G. and Lam, F. *Connections for Stackable Heavy Timber Modules in*
685 *Midrise to Tall Wood Buildings*. 2019, Timber Engineering and Applied Mechanics (TEAM)
686 Laboratory.
- 687 [25] Rothoblaas. *LOCK T: Concealed Hook Timber-to-timber Connector*. Available from:
688 [https://www.rothoblaas.com/products/fastening/brackets-and-plates/concealed-](https://www.rothoblaas.com/products/fastening/brackets-and-plates/concealed-connections/lock-t)
689 [connections/lock-t](https://www.rothoblaas.com/products/fastening/brackets-and-plates/concealed-connections/lock-t).
- 690 [26] Li, Z., Wang, X., He, M., Shu, Z., Huang, Y., Wu, A. *Mechanical performance of pre-*
691 *fabricated metal dovetail connections for Cross-Laminated Timber (CLT) structures*.
692 *Construction & building materials*, 2021. **303**: p. 124468.
- 693 [27] Fitzgerald, D., Miller, T.H., Sinha, A., Nairn, J.A. *Cross-laminated timber rocking walls*
694 *with slip-friction connections*. *Engineering structures*, 2020. **220**: p.110973.
- 695 [28] Fitzgerald, D., Sinha, A., Miller, T.H., Nairn, J.A. *Axial slip-friction connections for cross-*
696 *laminated timber*. *Engineering structures*, 2021. **228**: p.111478.
- 697 [29] Hashemi, A., Zarnani, P., Masoudnia, R., Quenneville, P. *Experimental Testing of Rocking*
698 *Cross-Laminated Timber Walls with Resilient Slip Friction Joints*. *Journal of structural*
699 *engineering*, 2018. **144**: p.4017180.
- 700 [30] Schneider, J., Tannert, T., Tesfamariam, S., Stiemer, S.F. *Experimental assessment of a*
701 *novel steel tube connector in cross-laminated timber*. *Engineering structures*, 2018. **177**: p.283-
702 290.
- 703 [31] Dires, S., Tannert, T. *Performance of coupled CLT shear walls with internal perforated*
704 *steel plates as vertical joints and hold-downs*. *Construction and Building Materials*, 2022. **346**:
705 p.128389.
- 706 [32] Kramer, A., Barbosa, A.R., Sinha, A. *Performance of Steel Energy Dissipators Connected*
707 *to Cross-Laminated Timber Wall Panels Subjected to Tension and Cyclic Loading*. *Journal of*
708 *structural engineering*, 2016. **142**(4): p. 4015013.
- 709 [33] Sarti, F., Palermo, A. and Pampanin, S. *Fuse-Type External Replaceable Dissipaters:*
710 *Experimental Program and Numerical Modelling*. *Journal of Structural Engineering* (New
711 York, N.Y.), 2016. **142**(12): p. 4016134.
- 712 [34] Hashemi, A., Zarnani, P., Masoudnia, R., Quenneville, P. *Seismic resistant rocking*
713 *coupled walls with innovative Resilient Slip Friction (RSF) joints*. *Journal of Constructional*
714 *Steel Research*, 2017. **129**: p. 215-226.
- 715 [35] Baird, A., Smith, T.J., Palermo, A., Pampanin, S. *Experimental and numerical Study of*
716 *U-shape Flexural Plate (UFP) dissipators*. In: 2014 NZSEE Conference. Auckland, New
717 Zealand; 2014.
- 718 [36] Xu, B.H., Taazount, M., Bouchaïr, A., Racher, P. *Numerical 3D finite element modelling*
719 *and experimental tests for dowel-type timber joints*. *Construction & Building Materials*, 2009.
720 **23**(9): p. 3043-3052.
- 721 [37] EN 12512:2001. *Timber Structures. Test methods. Cyclic Testing of Joints Made with*
722 *Mechanical Fasteners*. European Committee for Standardisation, 2005.
- 723 [38] EN 1380:2009. *Timber structures. Test methods. Load bearing nails, screws, dowels and*
724 *bolts*. European Committee for Standardisation, 2009.
- 725 [39] Sandhaas, C. *Mechanical behaviour of timber joints with slotted-in steel plates*. 2012,
726 Delft University of Technology: Netherlands.
- 727 [40] Sculpteo. *Steel/ Bronze 420SS/BR Material Guide*. Available from:
728 [https://www.sculpteo.com/en/materials/binder-jetting-material/binder-jetting-stainless-steel-](https://www.sculpteo.com/en/materials/binder-jetting-material/binder-jetting-stainless-steel-material/)
729 [material/](https://www.sculpteo.com/en/materials/binder-jetting-material/binder-jetting-stainless-steel-material/).
- 730 [41] EN ISO 6892-1:2016. *Metallic materials. Tensile testing. Method of test at room*
731 *temperature*. British Standards Institute, 2016.

- 732 [42] Doyle, M., Agarwal, K. Sealy, W., Schull, K. *Effect of Layer Thickness and Orientation*
733 *on Mechanical Behavior of Binder Jet Stainless Steel 420 + Bronze Parts*. Procedia
734 Manufacturing, 2015. **1**: p. 251-262.
- 735 [43] Hassanieh, A., Valipour, H.R. and Bradford, M.A., Sandhaas, C. *Modelling of steel-timber*
736 *composite connections: Validation of finite element model and parametric study*. Engineering
737 Structures, 2017. **138**: p. 35-49.
- 738 [44] Avez, C., Descamps, T., Serrano, E., Léoskool, L. *Finite element modelling of inclined*
739 *screwed timber to timber connections with a large gap between the elements*. European Journal
740 of Wood and Wood Products, 2016. **74**(3): p. 467-471.
- 741 [45] Tomasi, R., Crosatti, A. and Piazza, M. *Theoretical and experimental analysis of timber-*
742 *to-timber joints connected with inclined screws*. Construction & Building Materials, 2010.
743 **24**(9): p. 1560-1571.
- 744 [46] Liu, X., Bradford, M.A. and Lee, M.S.S. *Behavior of High-Strength Friction-Grip Bolted*
745 *Shear Connectors in Sustainable Composite Beams*. Journal of Structural Engineering, 2015.
746 **141**(6): p. 4014149.
- 747 [47] Dorn, M. *Investigations on the serviceability limit state of dowel-type timber connections*.
748 2012. Vienna University of Technology. PhD dissertation.
- 749 [48] Nassiri, S., Chen, Z., Lamanna, A., Cofer, W. *Numerical simulation of failure mechanism*
750 *in screw anchors under static tension*. Advances in Structural Engineering, 2020. **23**(16): p.
751 3385-3400.
- 752 [49] Bedon, C., and Fragiaco, M. *Numerical analysis of timber-to-timber joints and*
753 *composite beams with inclined self-tapping screws*. Composite Structures, 2019. **207**: p.13–28.
754
755

Highlights

- Detailed review of connection systems for Cross Laminated Timber volumetric structures.
- Development of an interlocking connection system for CLT volumetric structures.
- Finite element analyses on the translational behaviours of the proposed connection system.
- Monotonic and cyclic testing on 3D printed specimens demonstrates damage-control capacity of the proposed design.

Journal Pre-proof

Declaration of interests

The authors declare that they have no known competing financial interests or personal relationships that could have appeared to influence the work reported in this paper.

The authors declare the following financial interests/personal relationships which may be considered as potential competing interests:

Journal Pre-proof